7 Optical Parametric Oscillators

Norman P. Barnes
NASA Langley Research Center
Hampton, Virginia

1. INTRODUCTION

Optical parametric oscillators are a convenient method to create a widely tunable source of laser radiation. An optical parametric oscillator begins with a pump laser. In many cases the pump laser is a well-behaved solid-state laser such as a Nd:YAG laser or a frequency-doubled Nd:YAG laser. To complete the system, a nonlinear crystal between a set of mirrors is required. As such, the optical parametric oscillator by itself is an extremely simple device. Using an optical parametric oscillator, any wavelength longer than the pump wavelength and nominally within the transparency region of the nonlinear crystal can be created. However, practical problems limit the range of generated wavelengths to those that are somewhat longer than the pump wavelength, nominally a factor of 1.2 or so.

Optical parametric oscillators may be regarded as photon splitters. That is, a pump photon is split into two photons or one photon divides itself to create two photons. To satisfy conservation of energy, the sum of the energy of the two created photons must equal the energy of the pump photon. With the energy of a photon given by $h\nu$ where h is Planck's constant and ν is the frequency of the photon, the conservation of energy can be written as

$$\nu_1 = \nu_2 + \nu_3 \ . \qquad (1)$$

In this expression, the subscript 1 denotes the pump, 2 denotes the signal, and 3 denotes the idler. By convention, the signal is the higher of the two generated frequencies. Any pair of frequencies can be generated, but only frequencies that satisfy the conservation of momentum will be generated efficiently. Conservation of momentum can be expressed as

$$k_1 = k_2 + k_3 \ . \qquad (2)$$

In this expression, k_i is the wave vector at frequency ν_i. For the most common situation where the interacting beams are collinear, the vector relation simplifies to an algebraic relation. Substituting $2\pi n_i/\lambda_i$ for the wave vector, the relation becomes

$$n_1 \nu_1 = n_2 \nu_2 + n_3 \nu_3 \ , \qquad (3)$$

where n_i is the refractive index at the ith frequency. In practice, the conservation of momentum will limit the generated wavelengths to a relatively narrow spectral bandwidth.

Optical parametric oscillators have several desirable features including a wide range of tunability. In practice, the ultimate tuning range of the optical parametric oscillator is limited only by the conservation of momentum or the range of transparency of the nonlinear material. Consequently, the practical range of tuning is usually very wide and is set by the available transmission properties of the ancillary optics. Not only is the tuning range wide, the gain is relatively flat. To first-order approximation, the gain of the optical parametric device is maximized at the degenerate wavelength, which is where the signal and idler are equal. Away from the degenerate wavelength, gain decreases relatively slowly as the wavelength of the device is tuned to other wavelengths. Another advantage of this device is the inherent wavelength selectivity of the device. Although lasers with wide spectral bandwidths are available, several wavelength control devices are often used to effect the tuning. Optical parametric oscillators, on the other hand, have a built-in wavelength control mechanism, namely, the requirement to satisfy the conservation of momentum. Conservation of momentum does not provide fine wavelength control, but it does provide broad wavelength control.

Optical parametric oscillators have several other desirable features including a compact size, good beam quality, and the potential of high-gain amplifiers. A simple optical parametric oscillator consists of a nonlinear crystal in a resonator. As such, these devices can easily be hand-held items. In principle, the mirrors could be coated on the nonlinear crystal if a more compact device is required, however, this would limit the flexibility of the system. The beam quality of the device is usually good although it does depend on the beam quality of the pump laser. Heat loads on the optical parametric oscillator are usually quite small, thus minimizing the effects of thermally induced distortions on the beam quality. In addition, optical parametric amplifiers are available by simply deleting the mirrors forming the resonator. By utilizing optical parametric amplifiers, the output of an optical parametric oscillator can be amplified to the desired level. Optical parametric amplifiers are especially attractive because they are usually high-gain devices.

Optical parametric oscillators do require a pump laser often with good beam quality. Although optical parametric devices are usually compact, the size of the system does depend on the size of the pump laser. Because optical parametric oscillators are so small, the size of the system is essentially the size of the auxiliary pump laser. With the maturation of diode-pumped solid-state lasers, the size of the pump laser should decrease considerably. As optical parametric oscillators convert pump photons, the system efficiency is limited by the efficiency of the pump laser. In general, the evolution of diode-pumped solid-state lasers will also make a significant increase in the system efficiency. In addition to the limitations of the efficiency set by the efficiency of the pump laser, the optical parametric oscillator is limited by the ratio of the photon energy of the generated wavelength to the photon energy of the pump wavelength. For efficient systems, thus, the generated wavelength should be relatively close to the pump wavelength.

Although optical parametric oscillators have many desirable features, they have been limited in application to date primarily by the limited nonlinear crystal selection and the availability of damage-resistant optics. Even though nonlinear crystals have been investigated nearly as long as lasers themselves, the crystal selection was limited. However, a recent interest in these devices has been spurred by the introduction of several new nonlinear crystals, which have improved the performance of optical parametric oscillators. The efficiency of these devices is dependent on the power density incident on the nonlinear crystal. A high power density is required for efficient operation. Usually, the power density is limited by laser-induced damage considerations. Initially, the laser-induced damage threshold limited the performance of existing nonlinear crystals. However, some of the newer nonlinear crystals have demonstrated higher laser-induced damage thresholds. In addition, advances in optical fabrication and coating technology should further improve the laser-induced damage threshold. With these advances, optical parametric devices should become more efficient.

Optical parametric oscillators were demonstrated only a few years after the first demonstration of the laser itself [1]. For this demonstration, a *Q*-switched and frequency-doubled Nd:$CaWO_4$ laser served as a pump for a $LiNbO_3$ optical parametric oscillator. Tuning was accomplished by varying the temperature of the device, and the device was tuned between about 0.98 to 1.16 μm. However, the output power was low, about 15 W of peak power. From this initial demonstration, the state of the art has improved to where peak powers well above 1.0 MW are available and the tuning is limited essentially by the range of transparency of the nonlinear crystal.

Nonlinear optics devices in general and optical parametric oscillators in particular have received a significant amount of theoretical attention. Nonlinear interactions between three waves have been investigated by several authors [2,3]. In the first, the interaction between plane waves was considered. A treatment that allowed a variable phase between the interacting plane waves and also a depletion of the various waves provided a description where complete conversion could be achieved under ideal conditions. However, in reality, a plane wave is a mathematical fiction. Consequently, in the second of these treatments, the effects of a finite beam size were considered under the approximation of negligible depletion of the pump wave. In actual situations, the effects of both finite beam size and pump depletion should be taken into account.

A comprehensive review of the progress to date on optical parametric oscillators was given several years after the first introduction of the optical parametric oscillator [4]. In this review, the effects of Gaussian beams as well as the interaction were considered as well as the effects of singly resonant and doubly resonant optical parametric oscillator resonators. In addition, a calculation of the threshold pumping power was included and an estimate of the saturation and power output was given. A figure of merit to characterize the utility of nonlinear crystals was also introduced.

A later investigation of optical parametric oscillators focused on both the threshold and the linewidth of the device. Dependence of the threshold on the resonator length, the nonlinear crystal length, and the pump beam radius was measured and compared with the model developed to describe the operation of the device [5,6]. Linewidth was controlled by means of gratings, etalons, and the natural frequency-selective properties of the optical parametric interaction, including the aperture effect imposed by the finite pump beam radius. Combining these effects by using a square root of the sum of the squares technique, good agreement was obtained between the measured linewidth and the combination of the calculated linewidths. It has also been shown that calculations of the linewidths require an expansion of the phase mismatch including terms through second order [7].

Another treatment investigated the average power limit imposed on the optical parametric oscillator imposed by crystal heating that was caused by absorption of the interacting waves. Because absorption occurs throughout the volume of the nonlinear crystal while cooling occurs at the surface, thermal gradients within the nonlinear crystal are established. Because the refractive index depends on the temperature, phase matching cannot be maintained over the entire interaction volume. As the average power increases, the thermal gradients also increase, thereby limiting the volume over which the nonlinear interaction is effective. As the volume of the interaction decreases, the efficiency of the interaction also decreases. Average power limits have been estimated for the optical parametric interaction for both Gaussian and circular beam profiles [8].

2. PARAMETRIC INTERACTIONS

Optical parametric oscillators and amplifiers can be created by using the frequency mixing properties in nonlinear crystals. Nonlinearity in crystals can be characterized through a set of nonlinear coefficients. In general, the polarization of a crystal can be expanded in a power series of the applied electric field. For most materials, the components of polarization vector P_i are linearly related to the components of the applied electric field vector E_j. Subscripts refer to the vector components of the polarization and the electric field and are usually expressed in Cartesian coordinates. Nonlinear crystals have a significant nonlinear response to the electric field which can be described by

$$P_{i\,NL} = \epsilon_0 \sum_j d_{ij} (EE)_j \, . \tag{4}$$

where ϵ_0 is the permittivity of free space, d_{ij} are components of a 3 × 6 tensor, and $(EE)_j$ is the product of the applied electric fields creating the nonlinear polarization. Because the polarization depends on the product of the applied electric fields, frequency mixing can occur. That is, the product of the two electric fields will contain terms at both sum and difference frequencies. Sum and difference frequencies are obtained by expanding the product of two sine waves using trigonometric identities. Optical parametric oscillators use this effect to generate new frequencies or wavelengths from the pump.

Components of the nonlinear tensor depend on the symmetry of the nonlinear crystal. For a nonlinear crystal with very low symmetry, all 18 components of the nonlinear tensor may exist. However, in general, crystal symmetry reduces the number of independent components. Depending on the symmetry, some of the components are zero while other components may be simply related to each other. For example, some components may be equal to a given component or equal to the negative of a given component. Which components exist depends on the point group of the nonlinear crystal. Given the point group, the nonzero components and the relations between them can be determined by referring to tables [9].

To satisfy conservation of momentum, the nonlinear interaction usually occurs in a birefringent crystal. Over the range of transparency, the refractive index of a crystal is usually a monotonically decreasing function of wavelength. If this is the case, the crystal is said to have *normal dispersion*. Thus, in isotropic materials where there is only one refractive index, conservation of momentum cannot be satisfied. To satisfy conservation of momentum, a birefringent nonlinear crystal is utilized since, in these crystals, two indices of refraction are available.

In birefringent crystals the refractive index depends on the polarization, as well as the direction of propagation. In uniaxial birefringent crystals, at a given wavelength, the two refractive indices are given by [10]

$$n = n_o \; , \tag{5}$$

$$n = \left[\frac{\cos^2(\theta)}{n_o^2} + \frac{\sin^2(\theta)}{n_e^2}\right]^{-1/2} \; . \tag{6}$$

In this expression, n_o is the ordinary refractive index, n_e is the extraordinary refractive index, and θ is the direction of propagation with respect to the optic axis. For propagation normal to the optic axis, the extraordinary refractive index becomes n_e. Thus, the extraordinary refractive index varies from n_o to n_e as the direction of propagation varies from 0° to 90°. If there is a large enough difference in the ordinary and extraordinary refractive indices, the dispersion can be overcome and the conservation of momentum can be satisfied. A similar, but somewhat more complicated, situation exists in biaxial birefringent crystals.

Given the point group of the nonlinear crystal, an effective nonlinear coefficient can be defined. To calculate the effective nonlinear coefficient, the polarization and the direction of propagation of each of the interacting waves must be determined. Components of the interacting electric fields can then be determined by using trigonometric relations. If the signal and idler have the same polarization, the interaction is referred to as a Type I interaction. If, on the other hand, the signal and idler have different polarizations, the interaction is referred to as a Type II interaction. By resolving the interacting fields into their respective components, the nonlinear polarization can be computed. With the nonlinear polarization computed, the projection of the nonlinear polarization on the generated field can be computed, again using trigonometric relations. These trigonometric factors can be combined with the components of the nonlinear tensor to define an effective nonlinear coefficient. With a knowledge of the point group and the polarization of the interacting fields, the effective nonlinear coefficient can be found in several references [11]. Tables 7.2 and 7.3 tabulate the effective nonlinear coefficient for several point groups.

Given an effective nonlinear coefficient, the gain at the generated wavelengths can be computed. To do this, the parametric approximation is usually utilized. In the parametric approximation, the amplitudes of the interacting electric fields are assumed to vary slowly compared with the spatial variation associated with the traveling waves. At optical wavelengths, this is an excellent approximation. If, in addition, the amplitude of the pump is nearly constant, the equation describing the growth of the signal and the idler assumes a particularly simple form [12–14]:

$$\frac{\partial E_1}{\partial z} = -2\pi j \eta_1 \nu_1 d_e E_3 E_2^* \exp\left(-j\Delta k z\right) \; . \tag{7}$$

$$\frac{\partial E_3^*}{\partial z} = -2\pi j \eta_3 \nu_3 d_e E_1 E_2 \exp\left[-j\Delta k z\right] . \tag{8}$$

In these expressions E_i is the electric field, η_i is the impedance, ν_i is the frequency, d_e is the effective nonlinear coefficient, Δk is the phase mismatch, and j is the square root of -1. Subscripts 1, 2, and 3 refer to the pump, the signal, and the idler, respectively. Phase mismatch is the deviation from ideal conservation of momentum, or

$$\Delta k = 2\pi\left(\frac{n_1}{\lambda_1} - \frac{n_2}{\lambda_2} - \frac{n_3}{\lambda_3}\right) . \tag{9}$$

When the idler is initially zero and the signal is not, the coupled equations can be solved exactly to yield:

$$S_2 = S_{20}\left(1 + (\Gamma l)^2 \sinh^2\left[(\Gamma l)^2 - \left(\frac{\Delta k l}{2}\right)^2\right]^{1/2} \Big/ \left[(\Gamma l)^2 - \left(\frac{\Delta k l}{2}\right)^2\right]\right) . \tag{10}$$

In this expression, S_2 is the intensity of the signal, S_{20} is the initial intensity of the signal, l is the length of the nonlinear crystal, and

$$\Gamma = \frac{4\pi^2 d_e^2 |E_1|^2}{n_2 n_3 \lambda_2 \lambda_3} . \tag{11}$$

Although this expression describes the growth of plane waves well, in reality the interacting beams are not plane waves but are more likely to be Gaussian beams. When the interacting beams are Gaussian, the gain must be averaged over the spatial profile of the laser beam.

Two common approximations are available for this expression that demonstrate the limiting performance of parametric amplification. If the mismatch is small compared with the gain, that is, if Δk is much smaller than Γ, this term can be neglected. In this case

$$S_2 = S_{20} \cosh^2\left[\Gamma l\right] . \tag{12}$$

Thus, the signal will enjoy exponential gain as long as the pump is not depleted. On the other hand if the gain is small compared with the mismatch, that is, if Γ is much smaller than Δk, this term can be neglected. In this case,

$$S_2 = S_1\left[1 + (\Gamma l)^2 \sin^2(\Delta k l/2)/(\Delta k l/2)^2\right] . \tag{13}$$

In this case, energy can be transferred between the pump and the signal and idler beams and back again.

When a Gaussian beam enjoys a gain profile created by a Gaussian pump beam, an average-gain concept can accurately describe the situation. An average gain can be computed by integrating the product of the initial signal and the gain created by a Gaussian pump beam. With a Gaussian pump beam, the square of the electric field can be expressed as

$$|E_p|^2 = \frac{2}{c\epsilon_0 n_1}\frac{2P_1}{\pi w_1^2}\exp\left(\frac{-2\rho^2}{w_1^2}\right) , \tag{14}$$

where c is the speed of light, P_1 is the power of the pump beam, w_1 is the beam radius, and ρ is the radial coordinate. When the electric field of the pump varies with radial position, the gain also varies radially since Γ depends on the electric field of the pump. An average gain G_a can be defined as [15]

$$G_a = \int_0^\infty \frac{2}{\pi w_2^2}\exp\left(\frac{-2\rho^2}{w_2^2}\right)\cosh^2(\Gamma l)2\pi\rho d\rho . \tag{15}$$

Although this expression cannot be integrated in closed form, it is readily amenable to integration using numerical techniques. Note that this expression represents a power gain. Energy gain can then be readily computed by integrating this expression over time.

Gain in parametric amplifiers has been characterized experimentally and found to agree with the predictions of the model. For these experiments, a continuous wave (cw) HeNe laser operating at 3.39 μm was used as the signal, and a pulsed Er:YLF laser operating at 1.73 μm was used as the pump. Both the energy and the pulse length of the pump laser were measured to determine the power of the laser. Beam radii of both the pump and the signal beam were measured using a translating knife-edge technique. Pump energies ranged up to 15 mJ, and the pulse lengths, represented by τ_p, were typically around 180 ns. Even with this relatively low power, single-pass gains in excess of 13 were observed. In Fig. 1, the experimental gain of the signal versus $(E_p/\tau_p)^{1/2}$ is plotted along with the average gain computed from Eq. (15). To within experimental error, the agreement between the experiment and the prediction of the average gain is found to be reasonable. High single-pass gains available with optical parametric amplifiers make their use attractive in high-energy-per-pulse situations.

While high-gain optical parametric amplifiers are possible, amplified spontaneous emission (ASE) does not affect these devices like it affects laser amplifiers.

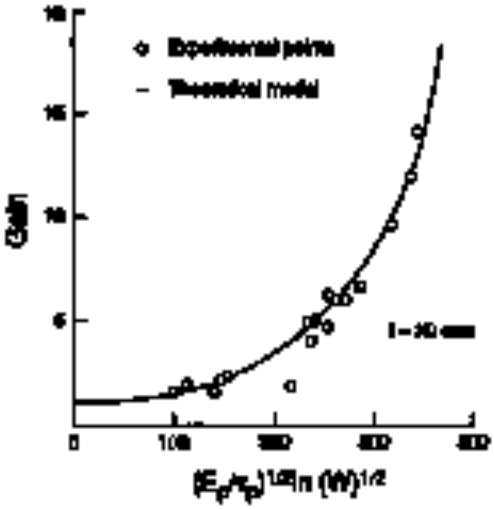

FIGURE 1 Average gain of 3.39-μm [illegible] laser as a function of pump power.

In a laser amplifier, energy is stored in the laser material for long time intervals, on the order of 100 μs. During this time interval, spontaneous emission can deplete the stored energy, thus reducing the gain. In an optical parametric amplifier, energy is not stored in the nonlinear material. In addition, gain is only present while the pump pulse traverses the nonlinear crystal, a time interval on the order of 10 ns or less. As such, ASE does not detract from the gain significantly.

3. PARAMETRIC OSCILLATION

Whereas parametric amplification occurs at any pump level, parametric oscillation exhibits a threshold effect. The threshold of a parametric oscillator can be determined for either pulsed or cw operation of the device. In a cw parametric oscillator, threshold will occur when gain exceeds losses in the resonator even though the time interval required to achieve steady state may be relatively long. In a pulsed parametric oscillator, on the other hand, gain may exceed the losses with no measurable output. In these cases, the pump pulse may become powerful enough to produce a net positive gain. However, before the generated signal reaches a measurable level, the pump power falls below the level at which positive gain is achieved. Consequently, to describe this situation both an instantaneous threshold and an observable threshold are defined. Pulsed gain is shown in Fig. 2 with a threshold set by the losses in the parametric oscillator resonator. Although an observable threshold depends on the detection system, it remains a useful concept. As the signal grows below observable threshold, it will enjoy

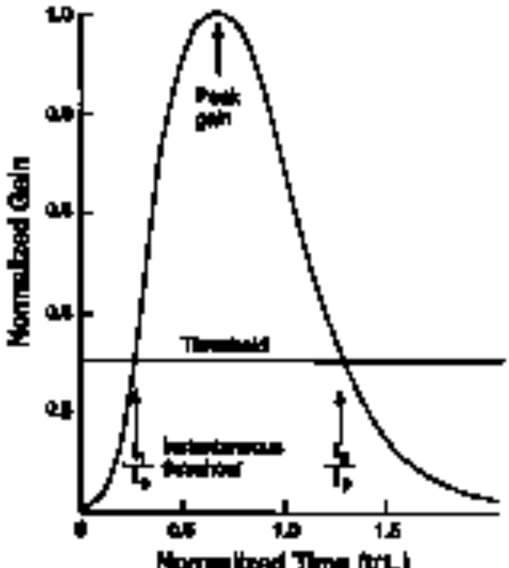

FIGURE 2 Pulsed gain as a function of time showing instantaneous threshold.

exponential gain. Because of this large gain, the difference between an observable threshold that produces 1.0 or 10.0 μJ is relatively small.

In the cw parametric oscillator, a small gain can be determined under threshold conditions. Because the pump beam will not be significantly depleted at threshold, the longitudinal variation of the pump beam may be neglected. Because the product of two Gaussian beams is another Gaussian beam, interacting beams will generate a nonlinear polarization, which is also a Gaussian. If the electric fields at wavelengths λ_i and λ_j interact, they will generate a nonlinear polarization at wavelength λ_k, which will have a spatial variation characterized by a beam radius given by

$$\frac{1}{w_k^2} = \frac{1}{w_i^2} + \frac{1}{w_j^2} . \tag{16}$$

Note that the generated nonlinear polarization does not necessarily have the same spatial variation as the incident field at λ_k. Because of the potential mismatch between the incident electric field and the generated electric field, the gain coefficient will have an additional term to account for this effect [6]. Including this term in the gain expression yields

$$(\Gamma l)^2 = \frac{8\pi^2 d^2 l^2 P_3}{n_1 n_2 n_3 \lambda_1 \lambda_2 \pi \epsilon_0} \frac{4}{\pi} \left(\frac{w_1 w_2 w_3}{w_1^2 w_2^2 + w_1^2 w_3^2 + w_2^2 w_3^2} \right)^2 . \tag{17}$$

Considerable simplification can result in this expression depending on whether the optical parametric oscillator is singly or doubly resonant.

In singly resonant oscillators, only one of the generated waves is resonant. Either the signal or the idler could be the resonant wave. In general, singly resonant oscillators are preferred for pulsed applications where the gain is high. In doubly resonant oscillators, both the signal and the idler are resonant. Doubly resonant oscillators are often used for cw applications because of the lower threshold. Doubly resonant oscillators are often more challenging to control spectrally because generated wavelengths must satisfy conservation of energy, conservation of momentum, and the resonance condition. If the parametric oscillator is a singly resonant device, only one of the generated waves has a beam radius determined by the configuration of the resonator. If, for example, the signal is resonant, the idler beam radius will be given by

$$\frac{1}{w_3^2} = \frac{1}{w_1^2} + \frac{1}{w_2^2} . \tag{18}$$

In this situation, the gain coefficient simplifies to

$$(\Gamma l)^2 = \frac{8\pi^2 d_e^2 l^2 P_1}{n_1 n_2 n_3 \lambda_2 \lambda_3 c \varepsilon_0} \, \frac{2}{\pi\left(w_1^2 + w_2^2\right)} . \tag{19}$$

A similar expression can be obtained if the idler is resonant by interchanging the subscripts. To maximize the gain, the pump beam radius and the resonant beam radius can be minimized. However, eventually laser induced damage or birefringence effects will limit the minimum practical size for the beam radii.

If the parametric oscillator is a doubly resonant device, both of the generated waves have a beam radius determined by the configuration of the resonator. To maximize the gain for a doubly resonant device, the beam radius of the pump can be optimized. Performing the optimization yields a beam radius for the pump, which is given by

$$\frac{1}{w_1^2} = \frac{1}{w_2^2} + \frac{1}{w_3^2} . \tag{20}$$

Utilizing the optimum pump beam radius yields a gain coefficient given by

$$(\Gamma l)^2 = \frac{8\pi^2 d_e^2 l^2 P_1}{n_1 n_2 n_3 \lambda_2 \lambda_3 c \varepsilon_0} \, \frac{2}{\pi\left(w_2^2 + w_3^2\right)} . \tag{21}$$

As in the case of the singly resonant oscillator, gain can be increased by decreasing the beam radii of the resonant beams. However, also as in the singly resonant device, laser induced damage and birefringence will limit the minimum size of the resonant beam radii.

Given the expressions for the gain, threshold can be defined by equating the gain and the losses. For cw operation, threshold will occur when [4]

$$\cosh\left(\Gamma l\right) = 1 + \frac{\alpha_2\alpha_3}{2-\alpha_2-\alpha_3} \ . \tag{22}$$

where α_2 is the round trip field loss at the signal wavelength and α_3 is the round trip field loss at the idler wavelength. In the singly resonant case and under small gain, α_2 is near unity and α_3 is near zero. Under these circumstances, the threshold for the singly resonant signal becomes approximately

$$\left(\Gamma l\right)^2 = 2\alpha_3 \ . \tag{23}$$

A similar expression exists for the situation where the signal is resonant. Again under the small-gain approximation but in the doubly resonant situation where both effective reflectivities are close to unity, the approximate expression for threshold becomes

$$\left(\Gamma l\right)^2 = \alpha_2\alpha_3 \ . \tag{24}$$

By employing a doubly resonant parametric oscillator, the threshold can be reduced substantially since α_2 can be an order of magnitude smaller than 2.0.

An observable threshold can be defined for pulsed parametric oscillators. An instantaneous threshold for a pulsed parametric oscillator is similar to the threshold for the cw case just defined. To define the observable threshold, Fig. 2 can be utilized. At time t_1, a net positive gain exists. At this time, the signal and the idler begin to evolve from the zero point energy. At time t_2 the pump power decreases to a point where the net gain is no longer positive. In the interim, as the signal and idler evolve, they are initially too small to be observed. For an observable threshold to be achieved, the power level in the resonant must increase essentially from a single circulating photon to a level that is accessible to measurement. To accomplish this, the gain must be on the order of exp(33).

Observable threshold depends on the time interval over which a net positive gain exists as well as how much the pump power exceeds the pump power required for threshold. For a circular pump beam, the observable threshold can be approximated by a closed-form expression [8]. In this approximation, a gain coefficient can be defined as

$$\left(\Gamma_0 l\right)^2 = \frac{8\pi^2 d^2 l^2}{n_s n_i n_p \lambda_s \lambda_i c\varepsilon_0}\,\frac{2E_p}{\pi w_p^2 \tau_1}\,\frac{2^{1/2}}{\pi} \, . \tag{25}$$

Using the gain defined in Eq. (25), the number of times over threshold, N, can be defined by using

$$\frac{1}{N} = \frac{-\ln\left(R_m T_c\right)}{2\Gamma_0 l} \, , \tag{26}$$

where R_m is the mean reflectivity of the mirrors at the resonant wavelength and T_c is the transmission of the nonlinear crystal. With these definitions, an observable threshold will be achieved at an approximate time when

$$33 = \frac{c\Gamma_0 N \tau_1}{l_c}\left[1 - \exp\left(\frac{-t^2}{\tau_1^2}\right) - \frac{2t}{N\tau_1} + \frac{2}{N^2}\right] . \tag{27}$$

In this expression, the pump pulse length τ_1 is related to the full width at half-maximum (FWHM) pulse length τ_{pr} through the relation

$$\tau_{pr} = 0.83\,\tau_1 \, . \tag{28}$$

If time t is less than the time at which the gain falls below the positive value, that is, t_2, an observable threshold will be achieved.

A slope efficiency can also be estimated for an optical parametric oscillator. Ultimately, the slope efficiency will be limited by the ratio of the photon energies. At best, each pump photon will produce a single photon at both the signal and idler wavelengths. Thus, the energy conversion efficiency will be limited by the ratio of the photon energy at the output wavelength to the photon energy at the pump wavelength; that is, the slope efficiency will be limited to λ_p/λ_s when the output is at the signal. In a singly resonant oscillator, in essence, all of the generated signal photons will be available for the output. However, for a doubly resonant oscillator, some of the generated photons will be dissipated by losses within the resonator. Consequently, for a doubly resonant oscillator, the ultimate slope efficiency will be limited by the ratio of the fractional output to the total losses in the resonator. If R_{2m} represents the output mirror reflectivity wavelength and R_{2l} represents the other losses at the signal wavelength, the ultimate slope efficiency will be further limited by the ratio of the output to the total losses, that is $\ln(R_{2m})/\ln(R_{2m}R_{2l})$. In many instances the losses in the parametric oscillator resonator can be kept small so that this ratio can be relatively high.

Experiments have demonstrated the validity of the basic approach [16,17]. For one set of experiments, an Er:YLF pump laser was used with a singly resonant

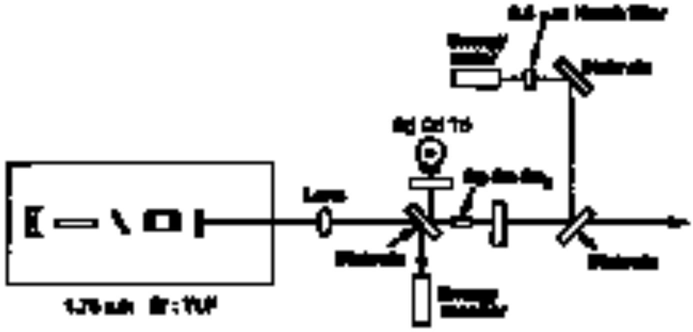

FIGURE 2 An $AgGaSe_2$ optical parametric oscillator experimental arrangement utilizing an Er:YLF pump laser.

$AgGaSe_2$ optical parametric oscillator. For these experiments, the signal was resonant rather than the idler, as shown in Fig. 2. The idler wavelength was 3.82 µm. A pump beam was introduced through a folding mirror within the optical parametric oscillator resonator. Output energy of the optical parametric oscillator was measured as a function of the pump energy for various lengths of the resonator. A typical plot of the results appears in Fig. 4. Data were extrapolated to define a threshold, and a slope efficiency was determined at an input energy 1.5 times the threshold.

Because the threshold depends on the number of passes the evolving signal can make through the gain medium, it can be reduced by decreasing the length of the parametric oscillator resonator. A shorter resonator length also improves the slope efficiency. By providing a shorter pulse evolution time interval, more of the pump pulse is available to be converted to useful output. Thus, both the threshold and the slope efficiency will benefit from a shorter resonator.

Benefits of a shorter resonator are displayed in Fig. 5. Data in this figure are presented for the same experimental configuration described previously. Threshold decreases, perhaps linearly, as the resonator length is decreased. For the shortest resonator length, the slope efficiency reaches 0.31. It may be noted that the ratio of the photon energies for this situation is 0.46. Thus, the observed slope efficiency is about 2/3 of the maximum slope efficiency.

4. SPECTRAL BANDWIDTH AND ACCEPTANCE ANGLES

Spectral bandwidth, acceptance angles, and allowable temperature variations are determined from the conservation of momentum or phase-matching condition. To satisfy the conservation of energy and momentum simultaneously requires a precise relation among the refractive indices at the various wavelengths. Referring to the previous section on parametric amplification, it can be shown that the efficiency of a low-gain and low-conversion nonlinear interaction

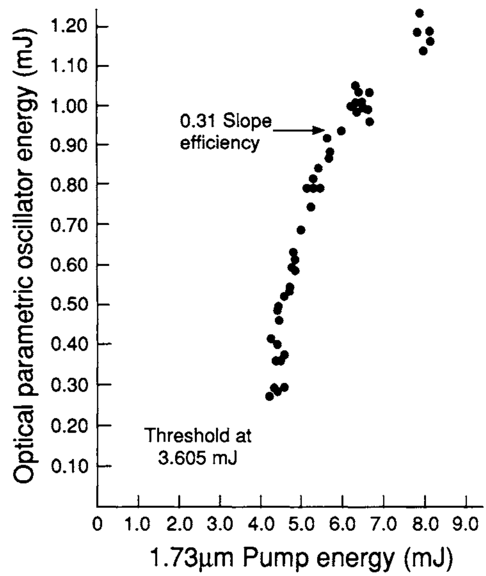

FIGURE 4 The $AgGaSe_2$ optical parametric oscillator output energy versus Er:YLF pump energy.

decreases according to a $\sin^2(x)/x^2$ relation. An allowable mismatch can be defined as

$$\Delta kl/2 = \pi/2 \ . \tag{29}$$

At this point, a nonlinear interaction decreases to about $(4/\pi^2)$ the efficiency of the ideally phase-matched interaction. For nonlinear interactions in the optical region of the spectrum, the ratio of the length of the nonlinear crystal to the wavelength is a large number. Thus to make the phase mismatch small, the relation among the three refractive indices becomes relatively strict. Because the refractive indices depend on the direction of propagation and temperature as well as the wavelengths, rather small variances are set for these parameters in order to satisfy the phase-matching condition.

Allowable variances for these parameters can be calculated by expanding the phase-matching condition in a Taylor series about the phase-matching condition. In general, if x is the parameter of interest, the mismatch can be expanded as follows [7]

$$\Delta k = \Delta k_0 + \frac{\partial \Delta k}{\partial x}\Delta x + \frac{1}{2}\frac{\partial^2 \Delta k}{\partial x^2}\Delta x^2 \ . \tag{30}$$

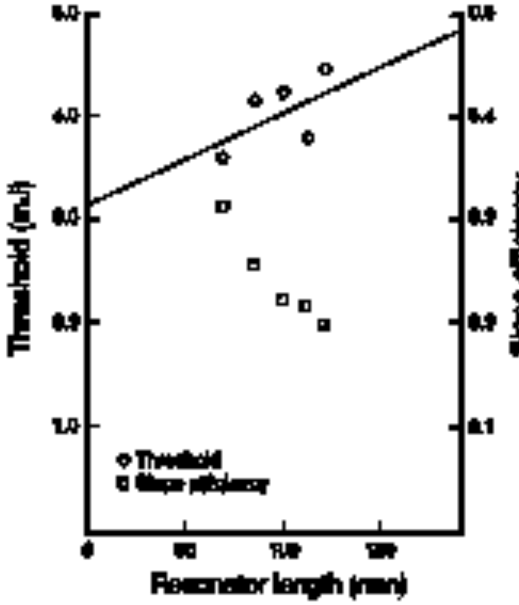

FIGURE 5 The $AgGaSe_2$ optical parametric oscillator threshold and slope efficiency versus resonator length.

By evaluating the expression at the phase-matching condition, the zeroth-order term vanishes. In most cases, the first term then dominates. When this is the case, the allowable variance of the parameter of interest is simply

$$\Delta x = \frac{\pi/l}{d\Delta k/dx} . \tag{31}$$

However, in many cases, the first-order term vanishes or is comparable to the second-order term. For example, the first-order derivative with respect to angle vanishes for noncritical phase matching. First-order derivatives with respect to wavelength can also vanish, often when the generated wavelengths are in the mid-infrared region [7]. In these cases, both the first- and second-order terms must be evaluated and the resulting quadratic equation must be solved to determine the allowable variance.

Acceptance angles should be calculated for orthogonal input angles. Consider the case where the ideally phase-matched condition defines a direction of propagation. For now, consideration will be restricted to uniaxial crystals. For the situation shown in Fig. 6 the ideally phase-matched direction and the optic axis of the crystal will define a plane referred to as the optic plane. For an arbitrary direction of propagation, two angles can be defined, one in the optic plane and the other orthogonal to the optic plane. In an uniaxial crystal, the refractive

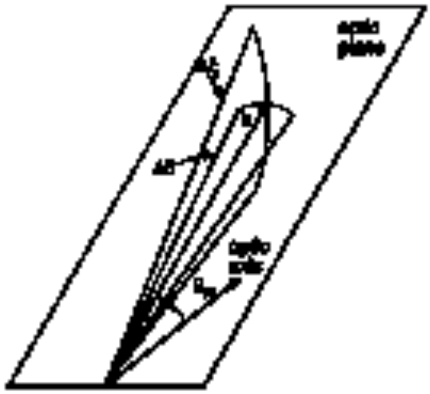

FIGURE 6 Definition of orthogonal acceptance angles for a uniaxial crystal.

index varies as the angle in the optic plane varies but is independent, to first order, of a variation of the angle orthogonal to the optic plane. In the optic plane, the derivative of the refractive index with angle is

$$\frac{\partial n}{\partial \theta} = \frac{n^3\left(n_o^2 - n_e^2\right)}{n_o^2\, n_e^2} \sin\left(\theta\right) \cos\left(\theta\right) . \tag{32}$$

Having evaluated the derivative of the refractive index with angle, the variation of the wave vector for extraordinary waves is

$$\frac{\partial k}{\partial \theta} = \frac{2\pi}{\lambda} \frac{\partial n}{\partial \theta} . \tag{33}$$

For ordinary waves, this derivative is, of course, zero. In most cases, the first-order derivative will dominate. As such, the acceptance angle will be determined using the first-order approximation. However, orthogonal to the optic plane, the first-order term vanishes. Here, the acceptance angle is determined by the second-order term. Usually, the first-order term will restrict the acceptance angle an order of magnitude more than the second-order term. First-order acceptance angles are often on the order of a few milliradians, comparable to the beam divergence of the laser in many cases. Because the second-order term is so much less restrictive, the acceptance angle orthogonal to the optic plane is often ignored. In biaxial crystals, the acceptance angles in orthogonal directions assume much more importance. In these crystals, the refractive index will, in general, depend critically on variations in the direction of propagation in both directions.

Measured acceptance angles agree well with the acceptance angles predicted using the preceding analysis. Although many examples are available, only ones will be presented [15]. Measurement of the acceptance angle can be performed using parametric amplifier experiments. Amplifier experiments can be used directly since the interacting wavelengths are fixed in these experiments. In parametric oscillator experiments, changing the angle at which the nonlinear crystal is oriented will tend to change the wavelength. As such, a measurement of the parametric oscillator output as a function of the orientation of the nonlinear crystal is likely to produce a tuning curve rather than a measurement of the acceptance angle. Data on the parametric amplifier presented here are for an $AgGaSe_2$ parametric amplifier pumped by a Ho:YAG laser. In this case, the $AgGaSe_2$ is ~20 mm in length and oriented at ~48° to the direction of propagation. A 3.39-μm HeNe laser is being amplified. Measured amplification as a function of the angular orientation of the crystal is shown in Fig. 7. Also shown is the predicted relative amplification as a function of the orientation of the crystal. To obtain the predicted relative amplification versus angle a relation of the form $\sinh^2[(\Gamma l)^2 - (\Delta k l/2)^2]^{1/2}/[(\Gamma l)^2 - (\Delta k l/2)^2]$ is used since the low-gain approximation is not valid in this case. Results of this experiment, as well as many others cited in the literature, tend to confirm the validity of this analysis.

The spectral bandwidth of the nonlinear interaction will be determined much like the acceptance angle in some respects. For optical parametric oscillators, the pump wavelength is usually fixed. However, as the signal wavelength varies, the idler wavelength can vary in order to satisfy conservation of energy or vice versa. Thus, a variation in one of these wavelengths will produce a corre-

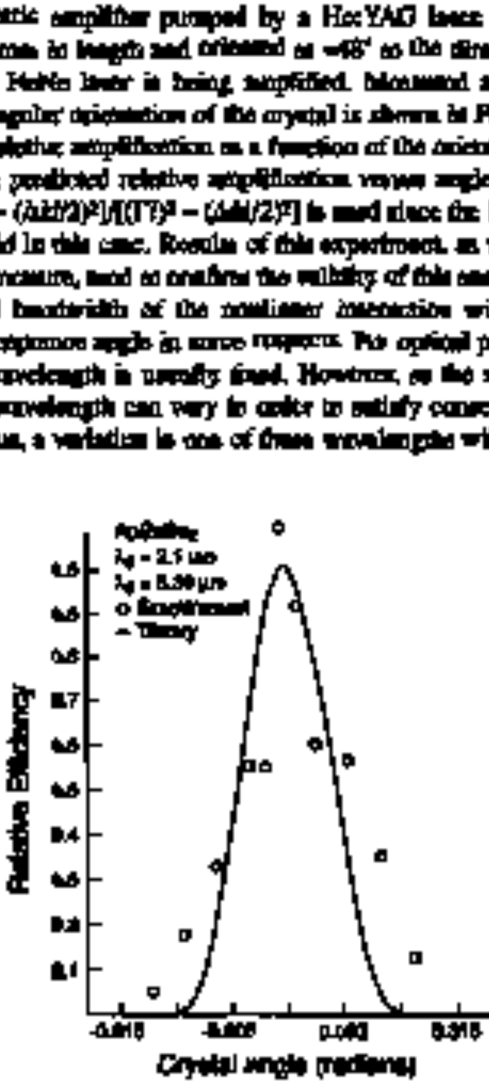

FIGURE 7 Measured acceptance angle.

pensating variation in the other wavelength. Keeping the pump wavelength fixed and taking the derivative of the mismatch with respect to the signal wavelength produces

$$\frac{d\Delta k}{d\lambda_s} = \frac{\partial \Delta k}{\partial \lambda_s} - \frac{\lambda_i^2}{\lambda_s^2}\frac{\partial \Delta k}{\partial \lambda_i} \ . \tag{34}$$

When taking the derivatives of the phase mismatch with respect to the wavelength, the pump wavelength can be considered to be fixed. Evaluating the partial derivatives in Eq. (34) yields

$$\frac{\partial \Delta k}{\partial \lambda_j} = \frac{2\pi}{\lambda_j}\frac{\partial n_j}{\partial \lambda_j} - \frac{n_j}{\lambda_j} \ . \tag{35}$$

Derivatives of the refractive index with respect to wavelength can be determined using experimental refractive index data or curve fits to the experimental refractive-index data. If a standard two-pole Sellmeier expression is used, then

$$\frac{\partial n}{\partial \lambda} = -\frac{\lambda}{n}\left[\frac{BC}{\left(\lambda^2 - C\right)^2} + \frac{DE}{\left(\lambda^2 - E\right)^2}\right] \ . \tag{36}$$

With these expressions, the single-pass spectral bandwidth of a difference-frequency interaction can be calculated.

To calculate the spectral bandwidth of an optical parametric oscillator, the number of passes of the signal through the nonlinear crystal must be taken into account. Calculated using equations 31 and 36 is the spectral bandwidth for a single pass. However, during the pulse evolution, the signal makes repeated passes through the nonlinear crystal. Subsequent passes through the nonlinear crystal will continue to narrow the spectral bandwidth of the parametric oscillator. It has been shown [17–19] that the spectral bandwidth depends on the number of passes the radiation makes through the spectral narrowing device, in this case the nonlinear crystal. To take this effect into account, the calculated single-pass spectral bandwidth should be divided by the $p^{1/2}$, where p is the number of passes that occur during the pulse evolution time interval. An estimate of the number of passes the signal makes through the nonlinear crystal can be obtained from the pulse evolution time interval τ_p using the relation

$$p = c\tau_p / 2l_c \ . \tag{37}$$

where c is the speed of light and l_c is the length of the parametric oscillator resonator.

The spectral bandwidth of the parametric oscillator depends on the spectral bandwidth of the pump laser as well as the spectral bandwidth of the interaction. Consider the situation in a singly resonant oscillator where, in addition, only a single resonant wavelength exists. If the pump laser consists of several wavelengths, each wavelength of the pump laser would mix with the single resonant wavelength of the parametric oscillator. As a result, each pump wavelength of the pump would produce a corresponding wavelength around the nonresonant wavelength. If $\Delta\lambda_3$ is the spectral bandwidth of the pump, the corresponding spectral bandwidth of the nonresonant wavelength is given by

$$\Delta\lambda_n = \Delta\lambda_3\, \lambda_n^2/\lambda_3^2 \; . \tag{38}$$

If the singly resonant oscillator does not restrict itself to a single wavelength but consists of a distribution of wavelengths with a spectral bandwidth of $\Delta\lambda_r$, then each resonant wavelength would mix with each pump wavelength to produce a corresponding wavelength around the nonresonant wavelength. In this case, the spectral bandwidth of the nonresonant wavelength can be approximated as

$$\Delta\lambda_n = \lambda_n^2 \left(\Delta\lambda_r^2/\lambda_r^4 + \Delta\lambda_3^2/\lambda_3^4\right)^{1/2} . \tag{39}$$

For equal spectral bandwidths of the pump and the resonant wavelength, the spectral bandwidth of the pump is weighted more heavily since the pump wavelength is shorter.

The spectral bandwidth of the parametric oscillator can also depend on the beam divergence of the pump. Heretofore, the phase mismatch has been expanded using a single variable. However, this parameter can be expanded as a function of two variables; for example, the wavelength and the propagation of direction. For each direction of propagation there is a combination of the signal and idler that minimizes the phase mismatch. Because a pump beam with finite divergence can be decomposed into a distribution of plane waves, each having a slightly different direction of propagation, a variety of wavelengths could result. To estimate this effect, the phase mismatch can be expanded in a Taylor series of two variables. Keeping terms only through first order and expanding around the ideal phase-matching direction yields

$$\Delta k = \frac{\partial \Delta k}{\partial \lambda}\,\Delta\lambda + \frac{\partial \Delta k}{\partial \theta}\,\Delta\theta \; , \tag{40}$$

where θ is an angle in the optic plane of an uniaxial crystal. For a beam with a divergence of $\Delta\theta$, the corresponding spectral bandwidth becomes

$$2\Delta\lambda = \frac{2(\partial\Delta k/\partial\theta)\Delta\theta}{\partial\Delta k/\partial\lambda} \; . \tag{41}$$

For TEM_{00} mode pump beams, the divergence internal to the nonlinear crystal is

$$\Delta\theta = \lambda_1 / n_1 \pi w_1 \quad . \tag{42}$$

Using this for the beam divergence and evaluating the partial derivatives, the magnitude of this effect can be estimated.

Experimental results appear in agreement with this analysis of the spectral bandwidth. The spectral bandwidths of parametric oscillators have been determined experimentally for several situations [17,18]. In one instance, a Nd:YAG pump laser was utilized with a $LiNbO_3$ parametric oscillator. In this study, the wavelength control exerted by the nonlinear crystal was compared with wavelength control exerted by other wavelength control elements such as gratings and etalons. In the other instance, an Er:YLF laser was used to pump an $AgGaSe_2$ optical parametric oscillator. In this study the effects of the pump divergence on the spectral bandwidth are compared with the effects of the pump spectral bandwidth and the spectral bandwidth of the nonlinear interaction. Results are shown in Fig. 8. It is of interest that in both cases the spectral bandwidth is significantly increased by the pump beam divergence.

An allowable variation of the temperature can also be defined in a similar manner by expanding the phase-matching condition as a function of temperature. Expanding the phase mismatch as a function of the temperature T yields

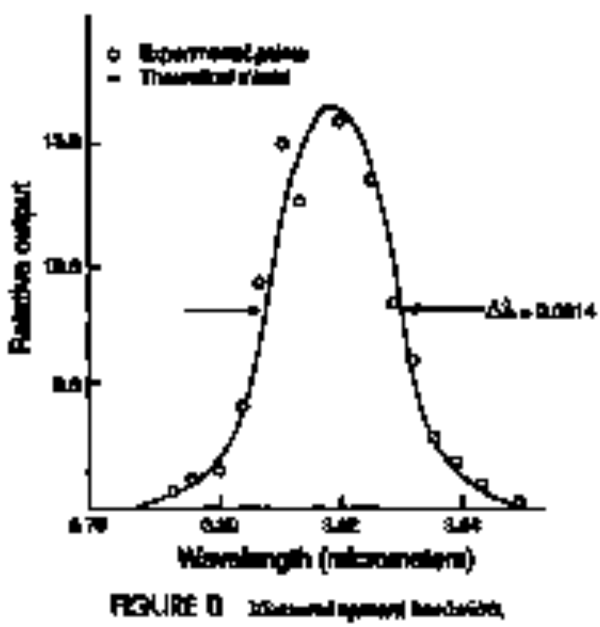

FIGURE 8 Measured spectral bandwidth.

$$\Delta k = \Delta k_0 + \frac{\partial \Delta k}{\partial T}\Delta T \ . \tag{43}$$

Expansion is usually limited to first order because the variation of the refractive index with temperature is usually known only to first order. Expanding the first-order term yields

$$\frac{\partial \Delta k}{\partial T} = 2\pi\left(\frac{1}{\lambda_1}\frac{\partial n_1}{\partial T} - \frac{1}{\lambda_2}\frac{\partial n_2}{\partial T} - \frac{1}{\lambda_3}\frac{\partial n_3}{\partial T}\right) \ . \tag{44}$$

For ordinary waves in uniaxial crystals, values for the variation of the refractive index with temperature can be used directly. For extraordinary waves, in general, the variation of the refractive index with temperature depends on the variation of the refractive index with temperature of both the ordinary and extraordinary waves. In uniaxial crystals this becomes

$$\frac{\partial n}{\partial T} = \frac{n^3\cos^2(\theta)}{n_o^3}\frac{\partial n_o}{\partial T} + \frac{n^3\sin^2(\theta)}{n_e^3}\frac{\partial n_e}{\partial T} \ . \tag{45}$$

Substituting these expressions into the allowable phase mismatch yields the allowable temperature variation. Allowable temperature variation also enters into the calculation of the average power limit for a nonlinear interaction as well as the temperature tuning rate.

5. BIREFRINGENCE EFFECTS

Even though birefringence is necessary to produce an efficient interaction by compensating for dispersion, birefringence will eventually limit the efficiency of the interaction. Efficiency limitations can arise since the direction of energy propagation of ordinary beams and extraordinary beams is not, in general, collinear in a birefringent crystal. Even when both the ordinary and extraordinary beams are normally incident on the birefringent crystal, a difference in the direction of the energy propagation exists. The direction of energy propagation of a normally incident ordinary beam does not suffer any deviation when entering the crystal. On the other hand, the direction of energy propagation of a normally incident extraordinary beam occurs at an angle to the normal, denoted by ρ. For non-normal angles of incidence, both the ordinary and extraordinary beams are deviated by refraction, in accordance with Snell's law. However, in addition, the extraordinary beam still experiences the effects of the birefringence, again characterized by the birefringence angle ρ. To satisfy the phase-matching condition, at least one of the interacting beams is an ordinary beam and at least one is an extraordinary beam. Thus, eventually the interacting beams separate, causing a decrease in the efficiency of the nonlinear interaction.

Birefringence angles can be calculated in uniaxial crystals given the ordinary and extraordinary indices of refraction, n_o and n_e, respectively [20]. In a given direction of propagation, there are two refractive indices for the two polarizations. Specifying a direction of propagation θ and the two refractive indices, denoted by n_o and n_e, a refractive index for the extraordinary polarized ray can be calculated, similar to the calculations used for phase matching. With these, the birefringence angle in an uniaxial crystal can be expressed as

$$\tan(\rho) = n'^{2}\left(n_o^{2} - n_e^{2}\right)\sin(\theta)\cos(\theta)\, n_o^{2}\, n_e^{2} . \tag{46}$$

In an uniaxial crystal, the angle ρ is measured in the optic plane. In a biaxial crystal, a similar analysis can yield the birefringence angle.

Birefringence eventually limits the region of overlap of interacting beams and therefore the efficiency of the nonlinear interaction. To obtain an estimate of the limitation, the region of the overlap can be calculated for the situation depicted in Fig. 9. Considering the overlap, an effective length l_e can be calculated by considering the following

$$l_e = \left| \frac{\int_{-\infty}^{\infty}\int_{-\infty}^{\infty}\int_0^{l} E_3 E_1 E_2 \, dx\, dy\, dz}{\int_{-\infty}^{\infty}\int_{-\infty}^{\infty} E_3 E_1 E_2 \, dx\, dy} \right|_{a} . \tag{47}$$

For extraordinary beams, the electric field can be represented as

$$E_i = \left(\frac{2}{\pi w_i^2}\right)^{1/2} \exp\left[\frac{-(x + \alpha z)^2 - y^2}{w_i^2}\right] . \tag{48}$$

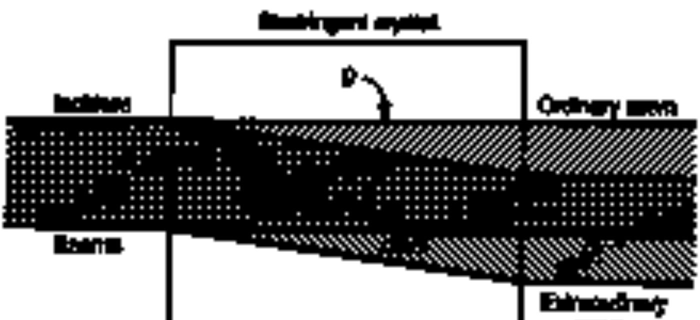

FIGURE 9 Birefringence effects.

where E_j is the electric field of the interacting wave and w_j is the beam radius. For ordinary waves, the expression for the electric field is similar but the birefringence angle is zero.

In the case of a singly resonant oscillator, an effective length for the nonlinear crystal can be calculated using the preceding expressions. As an example, consider the case where the signal is resonant. In this case, the beam radius of the nonresonant idler w_3 is given by

$$\frac{1}{w_3^2} = \frac{1}{w_1^2} + \frac{1}{w_2^2} . \tag{49}$$

With this nonresonant beam radius, the integral can be evaluated to obtain an effective length l_e for the oscillator crystal:

$$l_e = l_w \,\mathrm{erf}\left(\pi^{1/2} l / 2 l_w\right) . \tag{50}$$

Here, erf(x) is the error function and l_w is a parameter that depends on the beam radii of the pump beam and signal beam as well as birefringence.

In general, the parameter l_w is sensitive to which beams are ordinary and extraordinary as well as which waves are resonant and nonresonant. If the pump beam is an extraordinary beam and the signal and idler are both ordinary beams while the signal is resonant, l_w can be expressed as [21]

$$l_w = \frac{\pi^{1/2} w_1}{2\rho_1}\left(\frac{w_1^2 + w_2^2}{w_1^2 + w_2^2/2}\right)^{1/2} . \tag{51}$$

If the pump beam and the resonant wave are extraordinary waves, the expression for l_w becomes [8]

$$l_w = \frac{\pi^{1/2}}{2}\left[\frac{2w_1^2 + w_3^2\left(w_1^2 + w_3^2\right)}{w_1^2 + w_3^2\left(\rho_1^2 - \rho_1\rho_3 + \rho_3^2\right) + \rho_1^2 w_3^4 + \rho_3^2 w_1^4}\right]^{1/2} . \tag{52}$$

For other combinations of ordinary and extraordinary beams as well as resonant and nonresonant waves, the parameter l_w can be calculated using the same approach.

Because birefringence is needed to effect phase matching, but the birefringence angle essentially limits the effective length of the oscillator crystal, it is of interest to explore methods of achieving the former while minimizing the latter. One method of reaching this end is phase matching at 90° to the optic axis. If this can be effected, it is often referred to as noncritical phase matching. If noncritical phase matching is achieved, the birefringence angles become zero leading to an infinite effective length for the nonlinear crystal. In addition, the acceptance angle for the nonlinear interaction becomes much larger since the first-order term in the expansion of the phase mismatch vanishes. Since the ordinary and extraordinary indices of refraction have different dependencies on the temperature, noncritical phase matching may be possible by varying the temperature. However, if this is not possible, it is advantageous to select a nonlinear crystal that minimizes the deleterious effects of birefringence. Minimization can be accomplished by minimizing the difference in the ordinary and extraordinary index of refraction, that is, the birefringence, without compromising phase matching. Thus, it is of interest to determine how much birefringence is required.

An estimate of the required birefringence is dependent on the dispersion of the nonlinear crystal. Dispersion of the nonlinear crystal is characterized by the first derivative of the index of refraction with respect to the wavelength—∂n/∂λ. If the interacting wavelengths are far from the absorption edges of the nonlinear crystal, the dispersion can be approximated as being nearly independent of wavelength. As a natural extension of this, birefringence also tends to be independent of wavelength. Within these constraints, the required birefringence Δn can be estimated for the various types of interactions. For Type I interactions, the required birefringence can be approximated as

$$\left|\Delta n\right| = \left|n_e - n_o\right| \approx -\lambda_1 \frac{\partial n_1}{\partial \lambda} . \qquad (53)$$

For Type II interactions, a similar expression exists with the signal or idler wavelength replacing the pump wavelength, depending on which of these wavelengths has a different polarization compared to the pump wavelength. Birefringence in excess of this tends to limit the acceptance angle. In addition, more birefringence than required for phase matching exacerbates birefringence angle effects and thus the interaction length.

6. AVERAGE POWER LIMITATIONS

Thermally induced changes in the phase matching will limit the average power available from a nonlinear interaction. For all practical nonlinear crystals, significant absorption of the interacting wavelengths occurs even if the interacting waves are nominally in a transmitting region of the crystal. Absorption of the interacting wavelengths deposits heat throughout the volume of the nonlinear crystal. However, to dissipate the deposited heat, it must be conducted to the surface of the nonlinear crystal. Volumetric heating and surface cooling establish thermal gradients in the nonlinear crystal. Because the ordinary and extraordinary indices of refraction, in general, behave differently with temperature, the phase-matching condition cannot be maintained throughout the volume of the nonlinear crystal. As the average power increases, the generated heat and the concomitant thermal gradients increase. Consequently, the effective volume of the nonlinear crystal decreases, which, in turn, eventually limits the average power that can be produced.

Average power limitations will depend on the geometry of the nonlinear crystal and the interacting beams. When considering the geometry of the nonlinear crystal, actual cooling conditions in many instances can be approximated by two limiting situations. In most common situations, the lateral surfaces of the nonlinear crystal are in thermal contact with a heat sink while the entrance and exit surfaces are essentially insulated. In this case, the thermal gradients can be approximated as being radial. However, it is also feasible to insulate the lateral surface on the nonlinear crystal and extract the heat through the entrance and exit surfaces. Heat extraction could be accomplished by flowing a transparent fluid with high heat capacity over these surfaces. Gaseous He is an attractive candidate for such a fluid. In this case, the thermal gradients would be approximately along the direction of propagation of the beams or longitudinal. Both cases are depicted in Fig. 10.

Thermal gradients in the nonlinear crystal also depend on the beam profiles of the interacting beams. Again two approximations are commonly used. If the beam has a constant intensity out to some limiting radius and is essentially zero elsewhere, the beam profile is referred to as a circular beam profile. Such beam profiles can approximate beam profiles from laser resonators with graded reflectivity mirrors or from saturated amplifiers. If, on the other hand, the interacting beams are constrained to TEM_{00} modes, the beam profile is referred to as a Gaussian beam profile. Initially, the average power limit was calculated for a Gaussian beam profile and with lateral heat extraction [22]. However, similar analyses have been performed for several combinations of beam profiles and heat extraction methods [23].

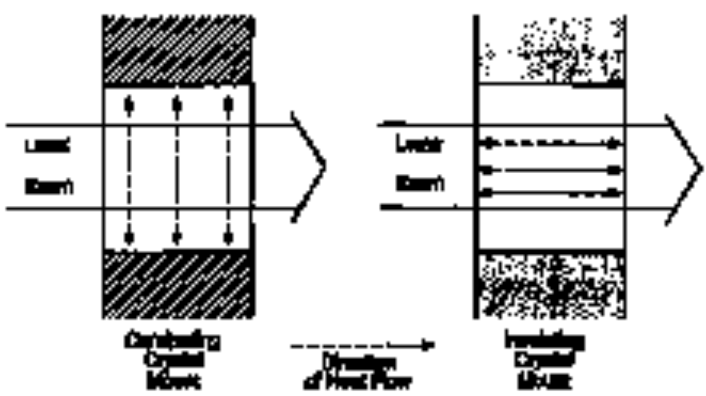

FIGURE 10 Heat flow in transversely and longitudinally cooled nonlinear crystals.

Under the assumption of radial crystal symmetry and small heat extraction, the phase mismatch can be approximated as a function of radial position, that is,

$$\Delta k = \Delta k_0 - a_{TC}\,\rho^2/w^2 \,, \tag{54}$$

$$\Delta k = \Delta k_0 - a_{TG}\left[1 - \exp\left(-\rho^2/w^2\right)\right] , \tag{55}$$

for a circular and a Gaussian beam profile, respectively. In these expressions a_{TC} and a_{TG} can be defined as

$$a_{TC} = \left(\frac{1}{\lambda_1}\frac{\partial n_1}{\partial T} - \frac{1}{\lambda_2}\frac{\partial n_2}{\partial T} - \frac{1}{\lambda_3}\frac{\partial n_3}{\partial T}\right)\frac{\beta_a P_A}{2k_c} \,, \tag{56}$$

$$a_{TG} = \left(\frac{1}{\lambda_1}\frac{\partial n_1}{\partial T} - \frac{1}{\lambda_2}\frac{\partial n_2}{\partial T} - \frac{1}{\lambda_3}\frac{\partial n_3}{\partial T}\right)\frac{\beta_a P_A}{k_c} \,, \tag{57}$$

In these expressions, $\partial n_i/\partial T$ is the variation with temperature of the refractive index n_i at wavelength λ_i, β_a is the average absorption coefficient, P_A is the average power, and k_c is the thermal conductivity. With the mismatch known as a function of the radial position, the conversion efficiency may be integrated over the cross section of the nonlinear crystal.

To explore this effect, a simple example can be investigated that illuminates the salient features. Effects of phase mismatch on parametric generation, under the low conversion efficiency approximation, can be described in terms of a $\sin^2(x)/x^2$ function. A relative efficiency η_R can be defined as the fractional decrease in the conversion efficiency caused by the effects of crystal heating. Integrating this over the cross section of the nonlinear crystal yields

$$\eta_R = \left(1/\pi w_c^2\right)\int_0^{2\pi}\int_0^{w_c} \sin^2\left(\Delta k l/2\right)/\left(\Delta k l/2\right)^2 \rho\, d\rho\, d\theta \,. \tag{58}$$

Evaluation of this integral is straightforward using numerical techniques. Referring back to the expressions for Δk, it can be seen that there are two contributions, a zeroth-order term that does not depend on the average power and another term that does. The zeroth-order term represents the residual phase mismatch in the absence of average power heating effects. For cases where there is no average power heating effects, the residual phase mismatch is minimized. However, with average power heating effects, this term may be optimized for maximum efficiency.

Relative efficiency can be calculated as a function of the heating parameter for the cases of no zeroth-order phase mismatch and optimum zeroth-order phase mismatch. A heating parameter ($al/2$) can be defined substituting the definitions of a_{rr} and a_{rz} for a. In this expression, l is the length of the nonlinear crystal. Relative efficiency is plotted in Fig. 11 for two cases, one where the zeroth-order term is zero and one where the zeroth-order term is optimized. A negligible zeroth-order phase mismatch would occur if the nonlinear interaction were optimized at a low average power and then the average power were increased. An optimized zeroth-order phase mismatch would occur when the nonlinear interaction were optimized at the final average power. Note that the optimum value depends on the value of the heating parameter. As can be seen in the figure, by using an optimum zeroth-order term the average power limit can be doubled. A similar calculation has been performed under the approximation of Gaussian beam profiles and the results are similar [23].

Average power limits depend on the absorption coefficients of the nonlinear crystal. Absorption coefficients depend on the wavelength; wavelengths nearer the transmission limits of the nonlinear crystal tend to be absorbed more

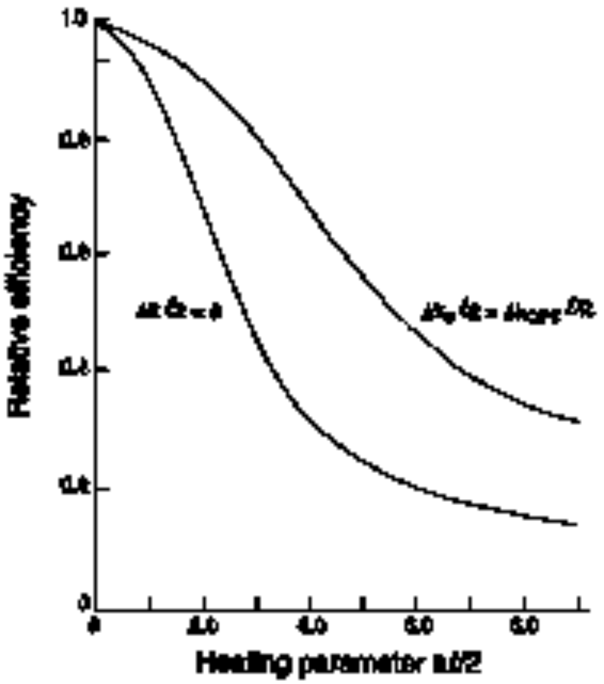

FIGURE 11 Relative efficiency versus heating parameter.

strongly. Absorption coefficients also depend strongly on purity of the crystal and the growth conditions. As such, the absorption coefficients can vary significantly from vendor to vendor and can also vary as a function of the date of purchase even if the crystals are from the same vendor. For many commercially available nonlinear crystals, absorption coefficients are on the order of 1.0 m^{-1} [24]. With absorption coefficients on this order, average power limits on the order of several watts appear feasible. However, optical materials with larger commercial demand can have significantly lower absorption coefficients. Because the heating parameter depends on the product of the average absorption coefficient and the average power, an order of magnitude decrease in the absorption implies an order of magnitude increase in the average power. Although absorption effects can impose practical limits, they can be mitigated through nonlinear crystal selection and crystal growth development efforts.

Pulse repetition frequency (prf) does not enter into the preceding estimate of the average power limit. As defined, the absorbed power which creates a thermal gradient large enough to limit the effective volume of the nonlinear crystal is estimated. If absorption of the pump power is the primary contributor to the heating, then the average power of the pump rather than the prf per se is the primary factor. However, if the absorption of the signal or idler is the primary contribution to the heating, then the prf can have more of an effect. With a constant average power and a high prf, the pump energy per pulse decreases. If this in turn decreases the conversion efficiency, less heating can occur. As such, as the prf increases, the average power heating decreases. However, the signal and idler power still decreases because of the lower conversion efficiency of even the ideally phase-matched interaction.

If even higher average power is required, the nonlinear crystal can be fabricated into a series of thin plates. The thin plates could be cooled by flowing gas between them. In essence, this decreases the thermal gradient by increasing the surface to volume ratio of the nonlinear crystal [25]. For a geometry like this, the longitudinal heat extraction technique is appropriate. While this technique will work, antireflection coatings on the surfaces will be required. A practical limit on the thickness of the plates will be set by the fabrication process.

7. NONLINEAR CRYSTALS

Many good nonlinear crystals are currently available for optical parametric oscillators and amplifiers and new nonlinear crystals are being developed constantly. In the early days of the development of optical parametric oscillators and amplifiers, only a relatively few nonlinear crystals were available. In addition, the available nonlinear crystals had limited utility either because of fundamental reasons or because of limited size and optical quality. Lack of good nonlinear crystals limited development of practical devices utilizing nonlinear crystals in these situations. Since then, many more nonlinear crystals have been discovered and the size and optical quality has improved. With continued improvements, optical parametric oscillators and amplifiers should find increasing use.

Selection of the best nonlinear crystal for a particular application depends on several basic crystal parameters including the transparency. In approximate order of consideration, the nonlinear crystal parameters that must be considered in the selection process include range of transparency, phase matching, nonlinearity, birefringence, and temperature sensitivity. The rationale for nonlinear crystal selection using these parameters is presented in some detail in the following paragraphs. Germane parameters, where available, are listed for select nonlinear crystals in Table I.

Transparency is an obvious requirement for the nonlinear crystal. However, it has been shown that a nonlinear interaction can occur even if one of the interacting waves is strongly absorbed [26]. Beyond the obvious, it is preferable to avoid the absorption edges of the crystal from an average power point of view. In addition, in cases where the crystal has limited birefringence, phase matching cannot be effected near either the ultraviolet or the infrared absorption edges since the absorption edges exhibit increased dispersion.

For efficient interactions, phase matching must be effected. Phase matching allows the entire length of the nonlinear crystal to contribute positively to the conversion efficiency. Nonlinear interactions can occur in situations where the phase-matching conditions can only be approximated by using plates cut to the coherence length. However, these situations require approximate phase matching in order to have reasonable lengths for the nonlinear crystal [27]. If approximate phase matching cannot be met, the coherence length and thus the nonlinear crystal length become short. In the low-conversion-efficiency regime, the conversion efficiency of a parametric interaction increases as the square of the length of the nonlinear crystal. Thus, phase matching must be possible in order to obtain long coherence lengths and the concomitant long nonlinear crystal lengths, and therefore reasonable efficiencies.

Efficiency of the optical parametric oscillator or amplifier also depends critically on the effective nonlinearity. Again in the low-conversion-efficiency regime, the conversion efficiency depends on the effective nonlinearity squared. Because the effective nonlinearity depends on the orientation of the nonlinear crystal, the effective nonlinearity is dependent on the phase-matching conditions and the interacting wavelengths. Inspection of the gain coefficient shows that the effective nonlinearity is divided by the refractive indices. Consequently, a commonly used figure of merit for nonlinear crystal selection is $d_e^2/n_1n_2n_3$. Often this figure of merit is plotted as a constant over the range of transparency of the nonlinear crystal. That is, the variation of the effective nonlinearity with wavelength is neglected. Because conversion efficiency is directly proportional to the figure of merit in the low-conversion approximation, a high figure of merit is desirable.

Effective nonlinear coefficients depend on the direction of propagation, polarization of the interacting wavelengths, and the point group. Given this

TABLE 1 Physical Properties of Selected Nonlinear Crystals[a]

Crystal	Point group	Transmission	Index	Variation of index	Thermal conduction
ADP *o*	42m	0.18–1.5	1.5065	−49.3	1.26
e			1.4681	≈0.0	0.71
KDP *o*	42m	0.18–1.7	1.4938	−34.0	1.34
e			1.4599	−28.7	1.21
CD*A *o*	42m	0.27–1.7	1.5499	−23.3	1.5
e			1.5341	−16.7	
$LiNbO_3$ *o*	3m	0.33–5.5	2.2340	0.2	4.6
e			2.1554	40.9	4.8
BBO *o*	3m	0.20–2.2	1.6551	−16.6	1.2
e			1.5426	−9.3	1.6
KTP *x*	mm2	0.35–4.5	1.7386	22.0	2.0
y			1.7458	25.9	3.0
z			1.8287	42.8	3.3
LBO *x*	mm2	0.16–2.3	1.5656	−1.9	3.5
y			1.5905	−13.0	3.6
z			1.6055	−8.3	
$AgGaS_2$ *o*	42m	0.50–13	2.4508	17.2	1.5
e			2.2924	18.3	1.4
$AgGaSe_2$ *o*	42m	0.71–18	2.7005	77	1.1
e			2.6759	45	1.0
CdSe *o*	6mm	0.75–20	2.5375	120	12.0
e			2.5572	141	
$ZnGeP_2$ *o*	42m	0.74–12	3.2324	204.9	35
e			3.2786	223.5	36
Tl_3AsSe_3 *o*	3m	1.30–13	3.3799	−45.2	1.8
e			3.1899	35.5	
Units		μm		10^{-6}/K	W/m K

[a]Refractive indices and the variation of the refractive indices with temperature evaluated at 1.064 μm except for TAS, which is evaluated at 2.1 μm. Thermal conductivities are quoted for the different crystallographic directions where available. In some cases, only a single value for the thermal conductivity was available.

information, the effective nonlinear coefficient can be obtained by decomposing the interacting electric field vectors into the coordinate system of the nonlinear crystal and performing the matrix multiplication indicated in the previous sections. However, this has already been done and the effective nonlinear coefficient

TABLE 2 Effective Nonlinear Coefficient for Uniaxial Crystals[a]

Point group	Interaction 001, 010, 100	Interaction 110, 101, 011
3	$(d_{11}\cos 3\phi - d_{22}\sin 3\phi)\cos\theta - d_{15}\sin\theta$	$(d_{11}\sin 3\phi + d_{22}\cos 3\phi)\cos^2\theta$
32	$d_{11}\cos\theta\cos 3\phi$	$d_{11}\cos^2\theta\sin 3\phi$
3m	$d_{15}\sin\theta - d_{22}\cos\theta\sin 3\phi$	$d_{22}\cos^2\theta\cos 3\phi$
4mm, 6mm	$d_{15}\sin\theta$	0
$\bar{4}$	$(d_{14}\sin 2\phi + d_{15}\cos 2\phi)\sin\theta$	$(d_{14}\cos 2\phi - d_{15}\sin 2\phi)\sin 2\theta$
$\bar{4}2m$	$d_{36}\sin\theta\sin 2\phi$	$d_{36}\sin 2\theta\cos 2\phi$
4, 6	$d_{15}\sin\theta$	0
$\bar{6}$	$(d_{11}\cos 3\phi - d_{22}\sin 3\phi)\cos\theta$	$(d_{11}\sin 3\phi + d_{22}\cos 3\phi)\cos^2\theta$
$\bar{6}m2$	$d_{22}\cos\theta\sin 3\phi$	$d_{22}\cos^2\theta\cos 3\phi$

[a] In this notation, 0 represents an ordinary wave and 1 represents an extraordinary wave.

TABLE 3 Effective Nonlinear Coefficient in Biaxial Crystals[a]

Point group	Plane	Interaction 001, 010, 100	Interaction 110, 101, 011
2	xy	$d_{23}\cos\phi$	$d_{36}\sin 2\phi$
	yz	$d_{21}\cos\theta$	$d_{36}\sin 2\theta$
	xz	0	$d_{21}\cos^2\theta + d_{23}\sin^2\theta - d_{25}\sin 2\theta$
222	xy	0	$d_{36}\sin 2\phi$
	yz	0	$d_{14}\sin 2\theta$
	xz	0	$d_{25}\sin 2\theta$
m	xy	$d_{13}\sin\phi$	$d_{31}\sin^2\phi + d_{32}\cos^2\phi$
	yz	$d_{31}\sin\theta$	$d_{13}\sin^2\theta + d_{12}\cos^2\theta$
	xz	$d_{12}\cos\theta - d_{32}\sin\theta$	0
mm2	xy	0	$d_{31}\sin^2\phi + d_{32}\cos^2\phi$
	yz	$d_{24}\sin\theta$	0
	xz	$d_{15}\sin\theta$	0

[a] In this notation, 0 represents an ordinary wave and 1 represents an extraordinary wave.

can be obtained by evaluating the expressions given in tables, such as Tables 2 and 3 [28,29]. For these tables, Kleinman's symmetry condition has been assumed. Values for the nonlinear coefficients of several common nonlinear crystals are found in Table 4 [30–32].

Kleinman's symmetry condition reduces the number of independent contributions to the nonlinear matrix and thus simplifies the expressions. Kleinman's symmetry condition assumes that the components of the nonlinear matrix which

TABLE 4 Nonlinear Coefficients for Selected Nonlinear Materials[a]

Crystal	Point group	Nonlinear Coefficients
ADP	$\bar{4}2m$	$d_{36} = 0.53$
KDP	$\bar{4}2m$	$d_{36} = 0.44$
CDA	$\bar{4}2m$	$d_{36} = 0.40$
$LiNbO_3$	3m	$d_{22} = 2.76$ $d_{31} = -5.44$
BBO	3m	$d_{22} = 2.22$ $d_{31} = -0.16$
KTP	mm2	$d_{31} = 6.5$ $d_{32} = 5.0$ $d_{33} = 13.7$
		$d_{24} = 7.6$ $d_{15} = 6.1$
LBO	mm2	$d_{31} = -1.09$ $d_{32} = 1.17$ $d_{33} = 0.065$
$AgGaS_2$	$\bar{4}2m$	$d_{36} = 13.4$
$AgGaSe_2$	$\bar{4}2m$	$d_{36} = 37.4$
CdSe	6mm	$d_{15} = 18.0$
$ZnGeP_2$	$\bar{4}2m$	$d_{36} = 75.4$
Tl_3AsSe_3	3m	$d_{22} = 16.0$ $d_{31} = 15.0$

[a]Units of the nonlinear coefficients are 10^{-12} m/V.

merely permute the subscripts are equal. Conditions where this is valid can be met in cases where the dispersion of the electronic polarizability is negligible. Such conditions exist in a majority of practical crystals. Assumption of this symmetry condition simplifies the expressions for the nonlinear coefficient.

Birefringence must be sufficient to achieve phase matching and adequate tuning but beyond that more birefringence is not usually desirable. A large birefringence usually indicates a restricted acceptance angle and a large birefringence angle. Both of these effects can limit the efficiency of the parametric interaction. However, there are instances where angular tuning rates can benefit from a large birefringence.

Temperature sensitivity arises through the variation of the refractive indices with temperature. Because, in general, the variations of the ordinary and the extraordinary refractive index with temperature are different, the phase-matching condition varies with temperature. If this difference is large, a small variation in the ambient temperature changes the phase-matching condition and adversely affects the efficiency. Thus, to maintain the efficiency, temperature control of the nonlinear crystal may be required. Although temperature control is straightforward it adds complexity to the system. In high-power situations, a large difference in the variation of the refractive indices adversely affects the average power limits of a given nonlinear interaction. On the other hand, a large difference in the variation of the refractive indices with temperature may allow 90°

phase matching to be effected with a concomitant increase in the acceptance angle and possibly in the efficiency.

Several of the available nonlinear crystals can be evaluated by considering the factors just outlined. Because of space limitations, such a survey cannot evaluate all of the known nonlinear crystals. Consequently, only a few select nonlinear crystals are evaluated here. More nearly complete surveys can be found in the literature. In general, the nonlinear crystals can be divided into two categories, depending on their range of transparency. Oxide crystals will generally transmit in the visible and near infrared while the semiconductor materials can transmit from the near infrared through much of the mid-infrared region. Tables 1 and 4 summarize the important properties of the select nonlinear crystals for facile reference.

ADP, or $NH_4H_2PO_4$, was one of the earliest nonlinear crystals to be used. ADP existed before lasers were invented and was useful because of its piezoelectric properties. As such, nonlinear crystals large enough for practical devices were available immediately. However, it does have relatively low nonlinear coefficients, a somewhat limited acceptance angle, and is hygroscopic. To avoid degrading the optical faces of a hygroscopic crystal by exposure to a humid atmosphere, it is often kept in a sealed container that may be heated. Because of the large difference in the variation of the refractive indices with temperature, ADP can be temperature tuned over a relatively large range. Even though several useful nonlinear devices have been demonstrated using this material, its use has been declining, primarily because of the availability of better materials.

KDP, or KH_2PO_4, was also available before the invention of the laser. KD*P, an isomorph where the hydrogen is replaced by deuterium, has nearly identical nonlinear coefficients and refractive indices but lower absorption in the near infrared, especially beyond about 1.0 µm. As such, KD*P is often preferred in cases where a high average power is required. Use of this material as a second harmonic generator for Nd:YAG lasers is common. However, like ADP, this crystal also has relatively low nonlinear coefficients and somewhat limited acceptance angle. KDP is also hygroscopic and therefore often kept in a crystal oven.

CD*A, or CsD_2AsO_4, is an isomorph of KDP and was developed primarily as a harmonic generator for Nd:YAG lasers. Its nonlinear coefficients are about the same as the previous two nonlinear crystals, but this material can achieve nearly noncritical phase matching for second harmonic generation of Nd:YAG lasers. Noncritical phase matching provides for a significantly enhanced acceptance angle and negligible birefringence angle effects. As with other KDP isomorphs, CD*A is hygroscopic.

$LiNbO_3$ was the first nonlinear crystal to demonstrate optical parametric oscillation. Nonlinear coefficients of this material are significantly larger than the previous three materials. However, this material suffered from optically induced refractive index inhomogeneities when irradiated with short-wavelength laser radiation. This deleterious effect can be mitigated by growing very pure materials, but it has not yet been eliminated. However, it has been discovered that this effect could be annealed out if the temperature were high enough. Annealing temperatures range from about 100 to 200°C, depending on the purity of the nonlinear crystal. Another option to avoid this effect was to confine operation to long wavelengths, roughly longer than 1.0 μm. $LiNbO_3$ displays a relatively large difference in the variation of the ordinary and extraordinary refractive indices with temperature making temperature tuning of nonlinear devices practical.

KTP, or $KTiOPO_4$, properties allow it to overcome many of the shortcomings of the previous nonlinear crystals. KTP has large nonlinear coefficients, and can be phase matched to have a large acceptance angle. It is a biaxial material, unlike the previous materials, which are all uniaxial. Being biaxial allows a greater variety of phase-matching conditions to be explored in order to find a larger effective nonlinear coefficient, a larger acceptance angle, or both. Its initial acceptance was hindered by the availability of sufficiently large crystals, a problem that has been largely ameliorated. Its ultraviolet absorption edge tends to limit the use of this crystal in the visible region.

BBO, or the β phase of BaB_2O_4, is a nonlinear crystal that is finding applications in the visible and near infrared. It has relatively large nonlinear coefficients, good transmission in the visible region, and its large birefringence allows phase matching throughout the visible region of the spectrum. However, this large birefringence leads to birefringence angle and acceptance angle problems in some cases. It does appear that this material is slightly hygroscopic.

LBO, or LiB_3O_5, is also a nonlinear crystal that will have applications in the visible region of the spectrum. It has similar transmission as BBO, but it does not display nonlinear coefficients as large as BBO. However, they are larger than those available with the KDP isomorphs. It does not suffer from the large birefringence angle effects of BBO and its biaxial nature allows a wider range of phase-matching conditions to be explored. It does not appear that this material is hygroscopic.

CdSe has a wide range of transparency in the mid-infrared region and is one of the first of the mid-infrared nonlinear crystals to be useful for optical parametric oscillator applications. CdSe has large nonlinear coefficients that allow efficient interactions to occur despite the fact that the interactions occur at longer wavelengths. However, it has a relatively low birefringence this can allow long interaction lengths, but not all desired interactions can be phase matched in this material.

$AgGaS_2$ is an interesting crystal for several reasons other than its nonlinear properties. Although it is birefringent, its birefringence vanishes at one particular wavelength in the visible. Vanishing of the birefringence has led to other applications such as optical filters. If near-infrared as well as mid-infrared transmission is desired, this nonlinear crystal is a good choice. It has large nonlinear coefficients, but not as large as $AgGaSe_2$. Consequently, the latter crystal is often selected in preference to this crystal except in cases where better visible and near-infrared transmission is desired.

$AgGaSe_2$ has large nonlinear coefficients but suffered initially from limited transmission in the near infrared. Absorption in the near infrared has been mitigated to a large extent by an annealing process. Because of the large vapor pressure of Se, this material often grows Se deficient. To overcome this, grown crystals have been annealed in Se-rich atmospheres. By doing this, the absorption in the near infrared is substantially reduced. Birefringence of this material is sufficient to effect phase matching but not so large as to impose severe acceptance angle problems. Both optical parametric oscillators and amplifiers have been demonstrated using this material.

$ZnGeP_2$ has an even larger nonlinearity than $AgGaSe_2$. It too suffers from absorption problems in the near infrared. As this material has a high vapor pressure during growth, an absorption analogy with $AgGaSe_2$ is possible. Several approaches to lowering this absorption have been tried with varying degrees of success. Birefringence of this material allows phase matching of a wide variety of nonlinearity interactions without incurring severe birefringence effects. In addition, this material has better thermal characteristics than $AgGaSe_2$.

TAS, or Tl_3AsSe_3, is a mid-infrared nonlinear crystal with sufficient birefringence to allow phase matching of a wide variety of nonlinear interactions. It has reasonably large nonlinear coefficients that have allowed its use as a nonlinear crystal. However, as mid-infrared nonlinear crystals with even larger nonlinear coefficients are available, this material also has seen somewhat limited use.

D. PHASE-MATCHING CALCULATIONS

Phase-matching curves are used to describe the orientation of the nonlinear crystal for which phase matching will be achieved. In uniaxial crystals, the angle for which phase matching is achieved is usually displayed as a function of the interacting wavelengths. In biaxial crystals, two angles are needed to describe the orientation of the nonlinear crystal. Consequently, phase matching can be achieved at a locus of points. Thus, for a given set of interacting wavelengths, the locus of the phase matching angles is usually described in terms of the polar and azimuthal angles. To determine the phase-matching angle or angles, the refractive indices of the interacting wavelengths must be determined.

A Sellmeier equation can be used to describe the variation of the refractive indices with wavelength. Historically several equations have been used to describe the variation of the refractive index as a function of wavelength. However, the Sellmeier equation has several advantages, including a physical basis and the ability to describe accurately the refractive index over relatively large wavelength intervals. Several forms of the Sellmeier equation have been reported, but the form that is most usually associated with a physical basis is expressed as

$$n^2 = A + B\lambda^2/\left(\lambda^2 - C\right) + D\lambda^2/\left(\lambda^2 - E\right) . \qquad (58)$$

In this expression, C represents the ultraviolet resonance wavelength squared and E represents the infrared resonance wavelength squared. In the same context, B and D represent the strengths of the ultraviolet and infrared absorption resonances, respectively.

If the ultraviolet or infrared resonances are not approached too closely, this form can represent the refractive index quite accurately. As the resonances are approached, effects such as the finite width of the resonance and the possibility of multiple resonances can detract from the accuracy. Typically, by adding a second ultraviolet resonance, the fit may be improved, especially as the ultraviolet resonance is approached. For example, the refractive index of Al_2O_3 has been accurately expressed using two ultraviolet resonances and an unity value for A [33]. However, away from the resonances, a nonunity value for A can be used to satisfactorily describe the refractive index without the added complexity of a double ultraviolet resonance.

Although the Sellmeier equation [given in Eq. (39)] has many desirable features, it is not universally utilized. However, to compute the refractive indices as well as the first and second derivatives of the refractive index with respect to wavelength, it is convenient to have a standard form for the expression relating the refractive index with the wavelength. Toward this end, original measurements of the refractive index as a function of wavelength were found and fitted to the standard form [34–44]. Results of the curve-fitting procedure are found in Table 3 for visible and mid-infrared crystals. In addition, the root mean square deviation between the calculated experimental values appears in Table 5. Typically, the experimental values are presented with four significant figures beyond the decimal point. Except for LBO, the root mean square deviation is in the fourth place after the decimal point. In cases where five significant figures were quoted in the cited literature (specifically ADP, KDP, and BBO), the fit is much better. The accuracy of this approach in describing the phase-matching angle has been demonstrated [17].

It is useful to have the temperature dependence of the refractive index built into the Sellmeier equation. With this feature, temperature tuning of the nonlinear interaction can be computed in a straightforward manner. In one case, this is possible since the refractive indices were measured accurately at two temperatures [36]. It is very convenient to have this information for $LiNbO_3$ because this nonlinear crystal is often operated at elevated temperatures when short wavelengths are among the interacting wavelengths. Operation of this nonlinear crystal at elevated temperatures helps control the optically induced refractive index inhomogeneities associated with the short wavelengths. If the material can be grown with close attention to the impurities, the optically induced refractive index inhomogeneities are annealed at about 105°C. Consequently, when a short-wavelength pump is used with this material, such as a 0.532-μm frequency-doubled Nd:YAG laser, the refractive indices associated with an elevated temperature should be used. Appropriate Sellmeier coefficients can be determined from the following relations.

$$A = 2.33907 + 4.20 \times 10^{-5}\,(T - 25)$$

$$B = 2.58395 - 10.47 \times 10^{-5}\,(T - 25)$$

$$C = 0.4588 + 1.13 \times 10^{-5}\,(T - 25)$$

$$D = 13.8109 + 7.73 \times 10^{-5}\,(T - 25)$$

$$E = 519.66$$

$$A = 2.39084 - 100.78 \times 10^{-5}\,(T - 25)$$

$$B = 2.22519 + 114.87 \times 10^{-5}\,(T - 25)$$

$$C = 0.04371 - 0.24 \times 10^{-5}\,(T - 25)$$

$$D = 13.9773 - 107.60 \times 10^{-6}\,(T - 25)$$

$$E = 741.15$$

for the ordinary and extraordinary Sellmeier refractive indices, respectively. In these expressions, temperature T is given in degrees centigrade. Operation at 105°C is only a small extrapolation of the refractive index data, taken at 25 and 60°C.

In cases where insufficient data are available for complete temperature-dependent Sellmeier coefficients, the variation of the ordinary and extraordinary refractive indices are given for selected wavelengths [35,37,41,45–47]. Far from the absorption features of the nonlinear crystal, the variation of the refractive index with temperature is relatively insensitive to the wavelength. Values for the variation of the ordinary and extraordinary refractive index with temperature are tabulated in Table 1.

Using the Sellmeier constants listed in Table 5, the phase-matching curves for Type I phase matching have been calculated for the selected uniaxial nonlinear crystals listed. For these calculations, pump wavelengths are 0.355, 0.532, 1.064, and 2.10 μm. Solid-state lasers make convenient pump sources for optical parametric oscillators because these lasers can operate either in a cw or a Q-switched mode. In particular, the Q-switched mode, with its short pulse lengths and concomitant high peak powers, is conducive to the operation of optical parametric oscillators and amplifiers. Pump lasers operating at these wavelengths can be obtained from a Nd:YAG laser and its harmonics or from either a Ho:Tm:Cr:YAG or Ho:Tm:Er:YLF laser. Phase-matching curves generated in this manner are not intended to be an exhaustive compilation of the possibilities but rather are intended to explore some of the more common situations. Other possible

TABLE 5 Sellmeier Coefficients for Selected Nonlinear Crystals[a]

Crystal	A	B	C	D	E	σ_{max}
ADP o	1.37892	0.91986	0.01206	-0.15071	5.7600	0.00905
e	1.37302	0.82752	0.01227	0.10512	3.3596	0.00814
KDP o	1.41344	0.86902	0.01229	0.26923	10.2590	0.00904
e	1.40472	0.72213	0.01204	0.07924	11.4890	0.00907
CD*A o	1.53975	0.75243	0.02514	0.06942	4.4890	0.00903
e	1.59748	0.65513	0.02768	0.04719	7.5095	0.00951
$LiNbO_3$ o	2.25907	2.62905	0.04985	13.8409	519.458	0.00921
e	2.25904	2.32510	0.05571	15.9773	741.349	0.00921
BBO o	1.71283	1.02795	0.01790	2.25118	138.650	0.00913
e	1.50289	0.88344	0.01312	0.36479	248.700	0.00904
KTP x	2.22751	0.79881	0.01706	0.07761	54.98	0.00937
y	1.90599	0.72272	0.05962	1.00978	97.30	0.00907
z	2.25706	0.96583	0.05818	1.24874	97.30	0.00951
LBO x	2.07597	0.39393	0.02908	2.60958	191.06	0.00951
y	1.81956	0.90047	0.01325	4.00956	204.86	0.00302
z	2.10372	0.30167	0.02176	2.35774	193.06	0.00907
$AgGaS_2$ o	3.02517	2.70048	0.08342	2.05965	910.301	0.00937
e	3.51263	2.22909	0.40048	2.04259	911.404	0.00951
$AgGaSe_2$ o	5.08904	2.76333	0.15690	11.72196	2902.6	0.00951
e	5.64502	2.23490	0.26902	8.54904	7894.4	0.00903
CdSe o	4.16922	1.83095	0.22148	2.48931	3640.06	0.00914
e	4.01216	2.87964	0.20309	13.8309	2106.12	0.00921
$ZnGeP_2$ o	4.54567	5.62067	0.13954	4.25777	1945.06	0.00948
e	4.71334	5.26856	0.14496	2.29310	1600.82	0.00948
Tl_3AsSe_3 o	1.0	9.473	0.19033	0.057	404.0	
e	1.0	6.703	0.19033	0.041	404.0	

[a] Wavelengths are in micrometers.

combinations can be obtained in a straightforward manner once the Sellmeier constants are known.

ADP, KDP, and CD*A can be used to generate output at wavelengths in the visible and near infrared, to about 1.1 µm or somewhat beyond. ADP and KDP are very similar, even to the shape of the phase-matching curve (Fig. 12). CD*A, on the other hand, does not have enough birefringence to be pumped by a 0.355-µm pump. However, by using a 0.532-µm pump, a parametric device tunable to wavelengths longer than about 0.85 µm is possible (Fig. 13). As phase matching can be obtained very near 90°, long nonlinear crystals may be employed without seriously affecting efficiency through the deleterious effects of birefringence.

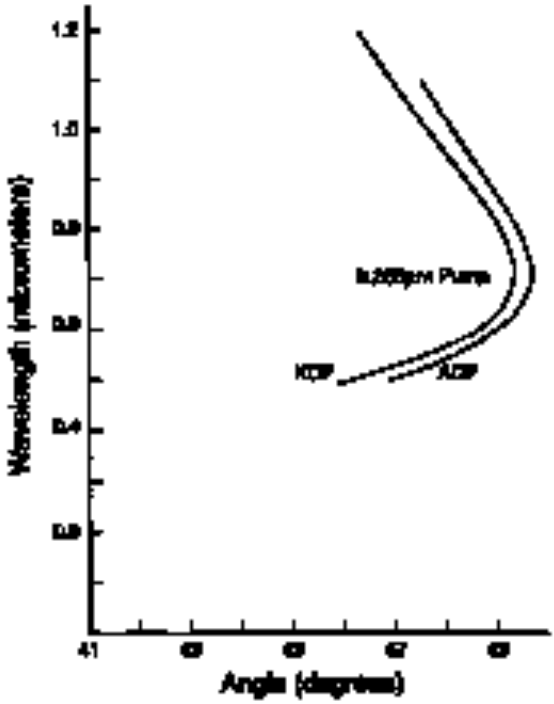

FIGURE 12 Phase-matching curves for ADP and KDP for a 0.266-µm pump.

Tunable radiation in the near infrared can be obtained from an optical parametric oscillator using a 0.532-µm pump and a $LiNbO_3$ or BBO nonlinear crystal (Figs. 14, 15, and 16). Operation at somewhat longer wavelengths than shown in the figures may be possible, depending on the infrared absorption properties of the particular nonlinear crystal. Because of absorption, calculations were not carried out beyond 2.2 µm in BBO and 4.0 µm in $LiNbO_3$. A device based on BBO would be attractive because a single crystal could be used to tune over a very large wavelength range. On the other hand, a device based on $LiNbO_3$ would be attractive if a narrow spectral bandwidth device were desired.

A Nd:YAG laser can be used directly as a pump source for at least three different nonlinear crystals, $LiNbO_3$, BBO, and $AgGaS_2$ (as shown in Figs. 15, 16, and 17). In the first case, the range from about 1.4 µm to beyond 4.0 µm could be covered with a single $LiNbO_3$ crystal. BBO could not cover the same range due to transparency limitations. On the other hand, $AgGaS_2$ could be tuned over a much wider range, from about 2.0 to beyond 10.0 µm. However, this tuning range would require a variation in the phase-matching angle of about 28°. Since the Nd:YAG laser has enjoyed a significant amount of development, such a system appears to be very attractive.

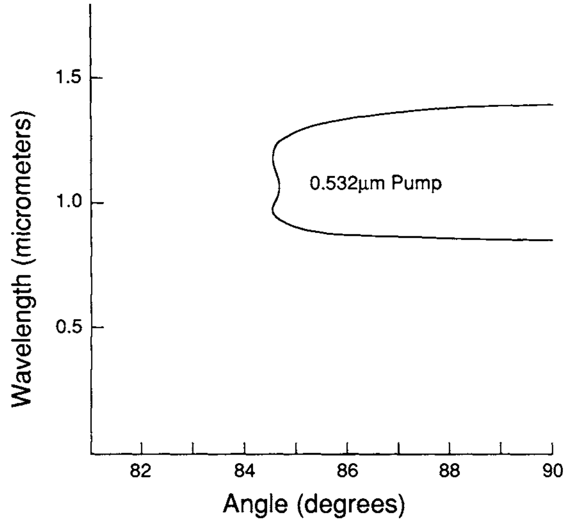

FIGURE 13 Phase-matching curve for CD*A for a 0.532-μm pump.

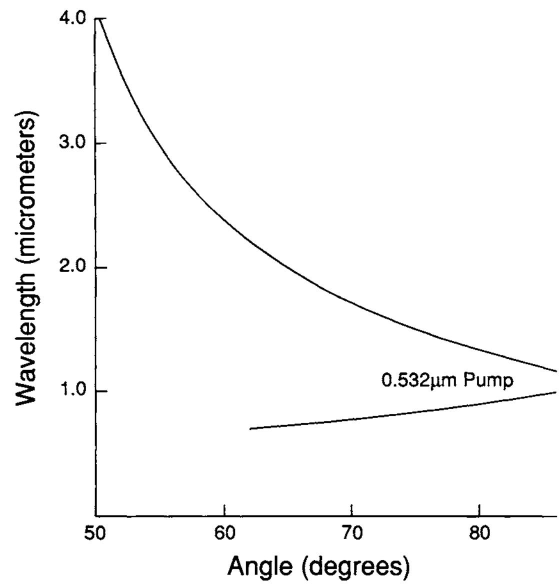

FIGURE 14 Phase-matching curve for $LiNbO_3$ for a 0.532-μm pump.

At least five different optical parametric oscillators can be made using a 2.10-μm pump. A device that could tune between about 2.5 μm to beyond 10.0 μm could be based on $AgGaS_2$, $AgGaSe_2$, CdSe, $ZnGeP_2$, or Tl_3AsSe_3 (Figs. 19

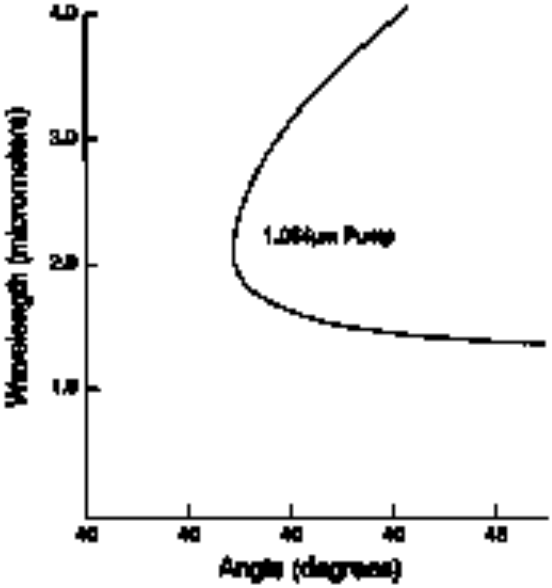

FIGURE 15 Phase-matching curve for $LiNbO_3$ for a 1.064-μm pump.

through 22). $ZnGeP_2$ could tune over this range with a variation of about 4°, the smallest angular range; CdSe would require about 14°, the largest angular range. $AgGaS_2$ does display an anomaly, the tuning range about 4.2 μm. Besides this, the tuning curves are in general similar, except for the direction of the curvature. As such, selection of the best nonlinear crystal would probably be based on considerations other than the phase matching curves.

9. PERFORMANCE

Optical parametric oscillators have developed from their initial stage where they were little more than a curiosity. Initial performance was limited by lack of high optical quality nonlinear crystals, nonlinear crystals with relatively small nonlinear coefficients, and limited pump laser performance. In addition, optical parametric oscillators were in competition with dye lasers in the visible and near infrared. Pulsed dye lasers have an advantage because laser-pumped dye lasers do not necessarily require high beam quality from the pump laser. In essence, dye lasers can serve as an optical integrator, converting a fixed-wavelength pump laser with relatively poor beam quality into a tunable laser with a better beam quality. In the face of these difficulties, optical parametric oscillators enjoyed limited commercial applications for a considerable time. However, several increases in optical parametric oscillator technology have improved the viability of these devices.

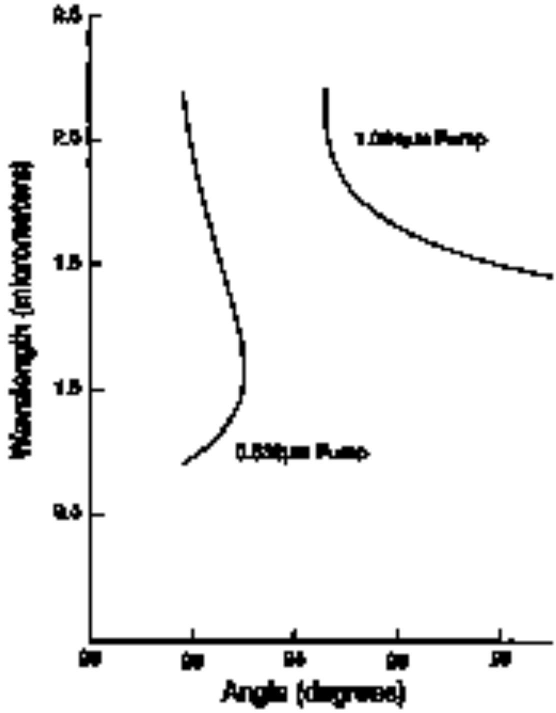

FIGURE 16 Phase-matching curve for BBO for 0.532- and 1.064-μm pumps.

Optical quality of the nonlinear crystals has improved. Optical quality improvements have occurred both in the form of decreased absorption and decreased distortion. For example, $LiNbO_3$ crystals were found to suffer from optically induced refractive index inhomogeneities. It was found that, in part, these problems could be traced to Fe impurities. By decreasing the Fe impurities, the susceptibility of optically induced refractive index inhomogeneities was decreased. Similarly, the short-wavelength absorption in $AgGaSe_2$ was correlated with a deficiency of Se. By annealing these crystals in an atmosphere rich in Se, the short-wavelength transmission of these crystals improved. Initially some nonlinear crystals were deliberately doped with impurities to reduce growth time and therefore cost. While some impurities are benign, others can cause unwanted absorption. Increased absorption can limit the efficiency and average power levels available with a given nonlinear crystal. In addition, some crystals tended to grow multidomain. That is, not all of the nonlinear crystal was oriented in the same manner. Multidomain crystals limit efficiency by limiting the effective length of the nonlinear crystal. As growth technology improved, many of these problems were resolved.

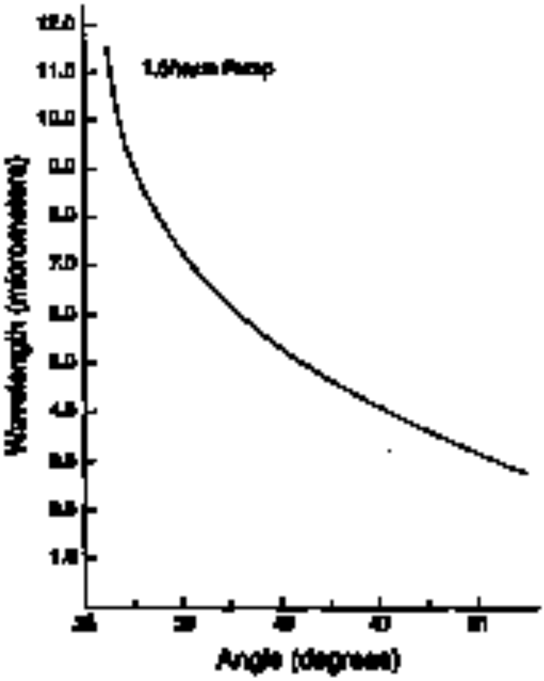

FIGURE 17 Phase-matching curve for $AgGaSe_2$ for a 1.064-μm pump.

Of perhaps more significance is the introduction of better nonlinear crystals, particularly ones with a larger nonlinear coefficient. Of particular note in the way of visible crystals are KTP, BBO, and LBO. Crystals with nonlinear coefficients as large as those available with these more recent crystals were not generally available in the early developmental stages of optical parametric oscillators. In the infrared, $AgGaSe_2$ has developed to the point where it is presently commercially available for applications in the mid-infrared region. Although this crystal has been known for some time, the availability and the absorption in the near-infrared region limited its utility. In addition, substantial progress has also been made with the commercialization of $ZnGeP_2$.

Pump lasers have also improved both in power and beam quality, a definite advantage when nonlinear optics are being used. Improvements such as unstable resonators and graded reflectivity output mirrors have made pump lasers with good beam quality as well as high energy per pulse available. The beam quality of pump lasers is often limited by thermal effects. However, as laser diode array pumping of solid-state lasers becomes more common, the beam quality should improve even more, since the thermal load for a laser diode array-pumped solid-state laser is less than a similar lamp-pumped solid-state laser at the same average output power. In addition, injection seeding techniques have narrowed the linewidth of the pump

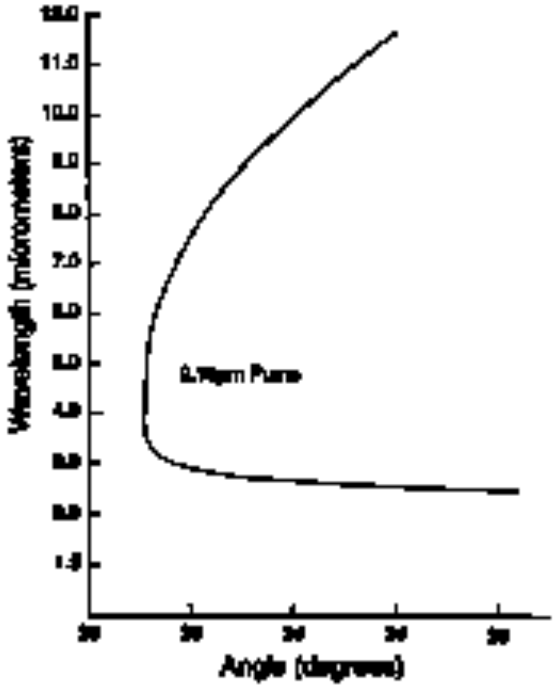

FIGURE 16 Phase-matching curve for $AgGaS_2$ for a 2.10-μm pump.

lasers. Both increased beam quality and decreased linewidth can lead to an increased performance for the optical parametric oscillator.

Several different concepts are involved in the assessment of the performance of an optical parametric oscillator including threshold, slope efficiency, total efficiency, photon efficiency, and pump depletion. Optical parametric oscillators can be operated either in a cw or a pulsed mode. Of the two modes of operation, the pulsed mode is much more common since the operation of an optical parametric oscillator is enhanced by a high power density. The threshold in the cw mode is straightforward to define as the amount of pump power required to achieve optical parametric oscillation. In the pulsed mode, the observable threshold, rather than the instantaneous threshold, is usually quoted; however, this is not always made clear. While slope efficiency is sometimes quoted, it could represent either the ratio of the increase in power at the output wavelength to the increase in power at the pump wavelength or the increase in power of both the signal and idler wavelengths to the increase in power at the pump wavelength. In the pulsed mode, it could be quoted as the increase of peak power or it could be quoted for the total output energy. Although laser theory usually predicts a nearly linear increase in the output with increases in the input, optical parametric oscillator theory does not necessarily predict the same approximation. However, in practice, a linear

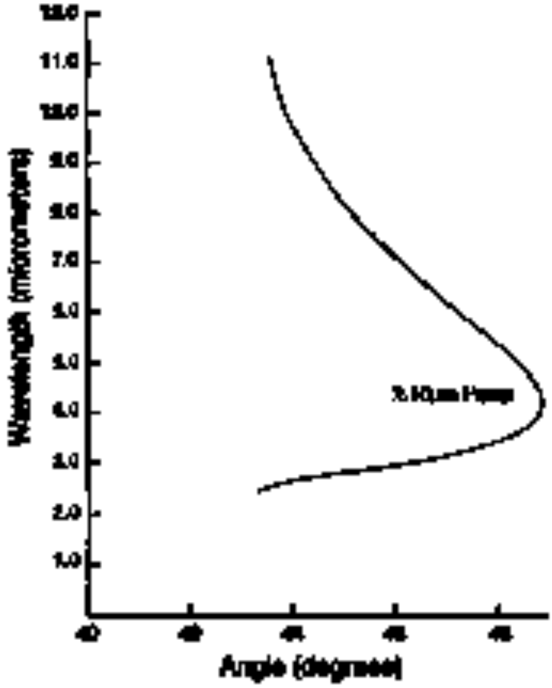

FIGURE 19 Phase-matching curve for $AgGaSe_2$ for a 2.10-μm pump.

increase of the output with the input is often observed. Total efficiency suffers from many of the same ambiguities as slope efficiency. It could imply the output power or energy at one or both of the signal and idler wavelengths divided by the pump power or energy. Photon efficiency normalizes the pump power and energy and the output power or energy by the energy of the pump and output photon, respectively. Thus, a unity photon efficiency would imply that the power or energy efficiency would be the ratio of the pump wavelength to the output wavelength. Pump depletion usually compares the pump pulse transmitted through the optical parametric oscillator with and without oscillation occurring. As such, it is closest to the efficiency calculated using both the signal and idler as outputs.

Optical parametric oscillation was first demonstrated using a pulsed pump laser, a frequency-doubled $Nd:CaWO_4$ laser [50]. The threshold was reported to be sharp and well defined at 6.7 kW, but was only achieved on about one in five shots. A peak output power of 15 W at a signal wavelength of 0.984 μm was reported, yielding an efficiency of about 0.002.

Continuous wave optical parametric oscillation was reported by using a $Ba_2NaNb_5O_{15}$ crystal [51]. It was pumped by a frequency-doubled Nd:YAG laser. A threshold of 45 mW was observed when the wavelengths available

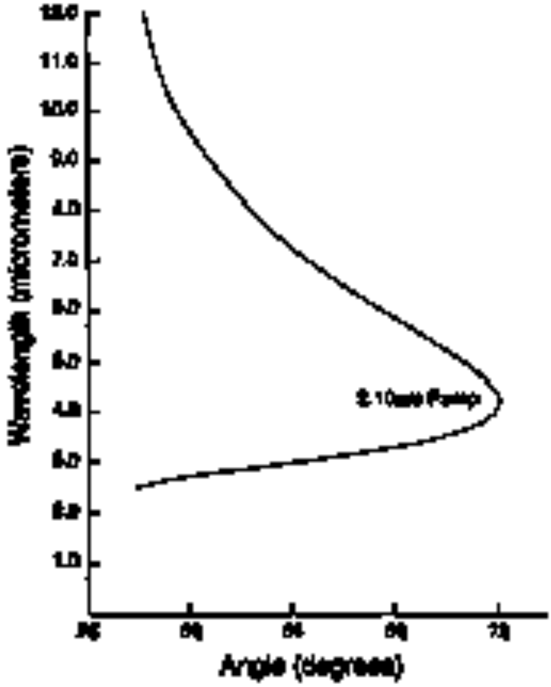

FIGURE 20 Phase-matching curve for CdSe for a 2.10-μm pump.

ranged from 0.98 to 1.16 μm. With 0.3 W of pump power, the available power at both the signal and idler wavelengths was estimated at 0.003 W, yielding an efficiency of 0.01. Later, by using a cw Ar ion laser for a pump laser, a threshold as low as 2.0 mW was achieved. A power output of about 0.0015 W was achieved at about 2.8 times threshold. While a continuous pump was employed, the output consisted of a series of pulses with pulse lengths ranging from 0.1 to 1.0 μs in length [52].

Most efficient operation in the near infrared was obtained by two experiments both using $LiNbO_3$ as the nonlinear crystal. In one case, a frequency-doubled Nd:glass laser was used as the pump source [53], and the other used a Q-switched $Cr:Al_2O_3$ laser [54]. In the first case, a threshold of about 3.0 kW was required for a 5.0-mm crystal length. At twice threshold, a peak output power of 1.9 kW was achieved yielding an efficiency of 0.12. In the second case a threshold of 65 kW was achieved in a doubly resonant arrangement with a 9.35-mm crystal length. With the doubly resonant arrangement, 0.22 of the peak pump power was converted to the signal at 1.04 μm. On the other hand, with a singly resonant arrangement, only 0.06 of the peak pump power was converted to the signal. Although the efficiencies reported in these experiments are impressive, the output energy of these devices is in the millijoule range or less.

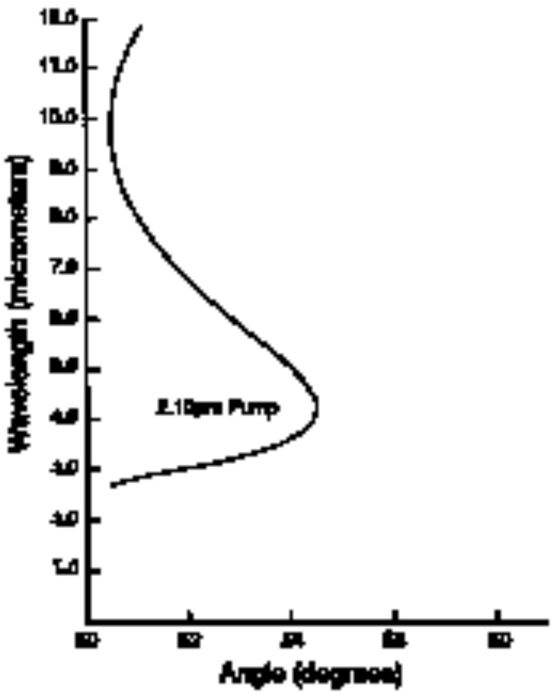

FIGURE 21 Phase-matching curve for $ZnGeP_2$ for a 2.10-µm pump.

A device tunable across the visible region of the spectrum was produced by using ADP as the nonlinear crystal [55]. A frequency-quadrupled Nd:YAG laser, yielding about 1.0 mJ/pulse at 0.266 µm, was utilized as the pump. Gains were high enough with this configuration that external mirrors were not necessary to obtain significant conversion. With the 50-mm ADP crystal oriented normal to the pump beam, an average power conversion of the pump to the outputs in the visible region of the spectrum was as high as 0.25. Temperature tuning the crystal from 50 to 105°C allowed the region from 0.42 to 0.73 µm to be covered.

A cw optical parametric oscillator tunable in the red region of the spectrum, from 0.680 to 0.705 µm, was demonstrated using an Ar ion laser operating at 0.5145 µm in conjunction with a 16.5-mm $LiNbO_3$ crystal [52]. To avoid optically induced refractive index inhomogeneities, the crystal was operated at elevated temperatures, nominally 240°C. A threshold of 410 mW was possible. At 2.8 times threshold, 1.5 mW of output power was available even though the output mirror only had a transmission of approximately 0.0004.

An optical parametric oscillator tunable in the mid-infrared region was obtained by using a Nd:YAG laser directly as the pump and a $LiNbO_3$ crystal [56]. Operation in this region of the spectrum is more difficult because the gain

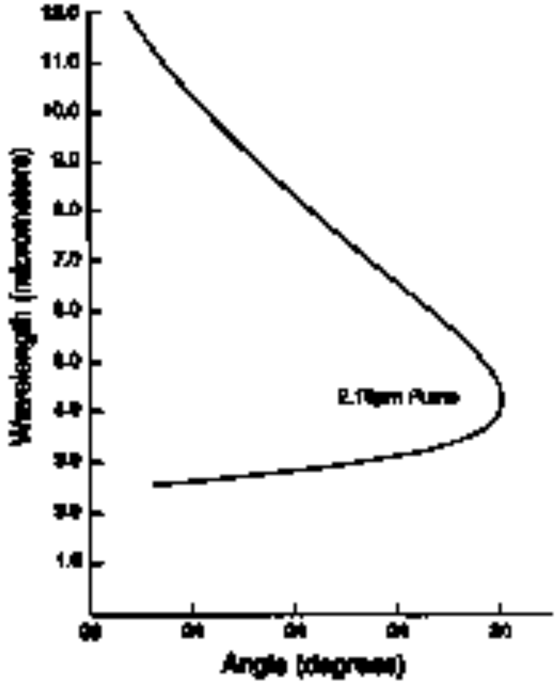

FIGURE 22 Phase-matching curve of Tl_3AsSe_3 for a 2.10-μm pump.

coefficient is inversely proportional to the product of the signal and idler wavelengths. To help compensate for the low gain, a 50-mm-long crystal was used. Using angle tuning, the spectral range from 1.4 to 4.5 μm could be covered. The threshold was 6.0 mJ when the oscillator was operating near 1.7 μm. An energy conversion efficiency of 0.15 was reported.

Optical parametric oscillation further into the mid-infrared region was possible by using a CdSe crystal. Initially, a Nd:YAG laser operating at 1.83 μm was used as the pump [57]. Later, a HF laser, operating around 2.87 μm was used for a pump [58]. In the former case, threshold for a 21-mm crystal length was observed to be between 0.55 and 0.77 kW. A power conversion efficiency of 0.40 was inferred by measuring the depletion of the transmitted pump. In the latter case, threshold for a 22-mm crystal length was found to be 2.25 kW. At about twice threshold, a signal power of 0.8 kW was observed that indicated a power efficiency of 0.15. By employing angle tuning, a signal was generated over the range from 4.3 to 4.5 μm. Corresponding to this, the idler was tuned between 8.1 to 8.3 μm.

Optical parametric oscillator operation can be enhanced by utilizing a mode-locked pump [59]. For one set of experiments, a mode-locked Nd:glass laser operating at 1.058 μm was amplified to produce an output of 0.55 J. By using an [illegible] in the Nd:glass laser resonator, the pulse length could change from 7 to 60 ps. Using a KDP crystal, this produced about 0.05 J of second harmonic. A $LiNbO_3$ crystal with a length of 20 mm was utilized as the nonlinear crystal. It was housed in an oven to allow temperature tuning. With the optical parametric oscillator tuned to 0.72 μm, an output of 6 mJ was achieved. To utilize the peak power associated with the pump, the length of the optical parametric oscillator had to be adjusted so that the circulating pulse was in synchronism with the incident pump pulse train. With a 7.0-ps pulse length, a change in the length of the resonator in the range of 0.1 mm produced a factor of 10 change in the output energy. In a different experiment, a mode-locked Ho:YAG laser was used to pump a CdSe optical parametric oscillator [60]. A similar enhancement in the conversion was effected by using the mode-locked pump pulse train.

An attractive optical parametric oscillator for use in the mid-infrared region was demonstrated using $AgGaSe_2$ as the crystal. Although CdSe could cover much of the mid infrared, its limited birefringence limited its tuning capability. However, much of the mid infrared could be covered using long-wavelength pump lasers including a 2.06-μm Ho:YLF [61] or a 1.73-μm Er:YLF [17] laser. Use of a 73-mm crystal length with the 1.73-μm pump resulted in a threshold of 3.6 mJ. A slope efficiency, measuring only the signal at 3.8 μm, of 0.31 at 1.5 times threshold was achieved simultaneously. On the other hand, with the 2.05-μm pump, a threshold of 4.0 mJ was achieved along with an energy conversion into both the signal and idler of 0.18.

Substantial energy conversion has been demonstrated using BBO as the nonlinear conversion by two different groups. Both groups used the third harmonic of a Nd:YAG as the pump. In one case, two opposed crystals, one 11.5 mm in length with the other 9.5 mm in length, were used to minimize birefringence angle effects [62]. Efficiency in this case is defined as the sum of the signal and idler energy output divided by the incident pump energy. Some significant saturation in the conversion efficiency was observed, nearly 0.32; that is, 7 mJ of output energy for 21 mJ of pump. In the other case, a 18-mm crystal length yielded a quantum conversion efficiency as high as 0.57 at a signal wavelength of 0.49 μm by double passing the pump through the nonlinear crystal [63].

By simply using more energetic pump lasers, more output energy can be obtained. By using a Nd:YAG oscillator and amplifier a pump energy of about 0.35 J/pulse could be obtained. Using two opposed KTP crystals 10 mm in length, for birefringence angle compensation, a nearly degenerate optical parametric oscillator was demonstrated [64]. Signal and idler wavelengths were 1.98 and 2.31 μm, respectively. The threshold for this arrangement was about 100 mJ and the slope efficiency was as high as 0.46. At the full input energy, 0.115 J/pulse was produced. Even higher energy per pulse could be obtained by simply scaling the device in cross section while retaining the same energy density.

10. TUNING

Tuning of the optical parametric oscillator can be handled using the same techniques as described in the chapter on solid-state lasers (Chapter 6; see also Chapter 2). However, significant differences do exist that can be attributed to the differences in the operating principles of the two devices. Some of these differences are manifest in the coarse tuning available with phase matching of the optical parametric oscillator and in the time-varying bandwidth, which has to be taken into account if injection seeding is to be utilized. However, because many of the tuning and line narrowing elements are discussed in Chapter 6, they will not be discussed here. Rather, the tuning aspects unique to the optical parametric oscillator will be emphasized.

Coarse tuning of the optical parametric oscillator can be accomplished using either angular or temperature tuning. In fact, any effect that causes a differential change in the refractive indices at the pump, signal, and idler wavelengths could be used to effect tuning. For example, tuning could be achieved using an applied pressure through the stress optic effect. However, to date, only angular or temperature tuning has received wide application. To calculate the tuning rate, the partial derivatives of the phase mismatch can be used. According to a theorem in partial differential calculus,

$$\frac{\partial x}{\partial y}\bigg|_z \frac{\partial y}{\partial z}\bigg|_x \frac{\partial z}{\partial x}\bigg|_y = -1 \ . \tag{60}$$

Using this relation, the tuning rate can be approximated by

$$\frac{\partial \lambda}{\partial \theta} = -\frac{\partial \Delta k/\partial \theta}{\partial \Delta k/\partial \lambda} \tag{61}$$

for angular tuning and

$$\frac{\partial \lambda}{\partial T} = -\frac{\partial \Delta k/\partial T}{\partial \Delta k/\partial \lambda} \tag{62}$$

for temperature tuning. To evaluate the derivatives of Δk with respect to the direction of propagation and temperature, the results of Sec. 4 can be used. Thus,

$$\frac{\partial \Delta k}{\partial \theta} = 2\pi\left(\frac{1}{\lambda_3}\frac{\partial n_3}{\partial \theta} - \frac{1}{\lambda_1}\frac{\partial n_1}{\partial \theta} - \frac{1}{\lambda_2}\frac{\partial n_2}{\partial \theta}\right) \tag{63}$$

in general. Of course, the partial derivative with respect to angle for ordinary waves is zero in uniaxial crystals. For temperature tuning,

$$\frac{\partial \Delta k}{\partial T} = 2\pi\left(\frac{1}{\lambda_1}\frac{\partial n_1}{\partial T} - \frac{1}{\lambda_2}\frac{\partial n_2}{\partial T} - \frac{1}{\lambda_3}\frac{\partial n_3}{\partial T}\right) \tag{64}$$

Individual partial derivatives with respect to angle are evaluated in Section 4. Partial derivatives of the index of refraction with respect to temperature are listed for the more common crystal in Section 8. Thus, to determine the particular wavelength that will be generated, the phase-matching condition can be calculated as done for a variety of situations in Section 8. Tuning near the phase-matching condition can then be found by using the preceding equations. Linewidth can be determined by using the approach also described in Section 4.

Injection seeding of an optical parametric oscillator can be accomplished in much the same way as injection seeding of a solid-state laser. Injection seeding has been demonstrated for several optical parametric oscillators operating in the visible and mid-infrared regions [65–67]. However, there are several significant differences between seeding an optical parametric oscillator and injection seeding a solid-state laser [67]. One of these differences occurs during the critical pulse evolution time interval. During this phase of the development, not much energy is extracted. However, the spectral properties of the output are determined by the competition between the seeded and unseeded modes. In a solid-state laser, the gain is nearly constant since the stored energy or the population inversion density is nearly constant. In an optical parametric oscillator, the gain varies with the pump power. Thus, for a pulsed pump, the gain varies with time. Although this makes the description of the competition more complex, it does not prevent seeding. A second difference is in the extraction of the energy. In a solid-state laser, as the seeded mode extracts the energy stored in the upper laser level, it hinders the development of the unseeded mode by decreasing the gain. However, in an optical parametric oscillator, there is no stored energy. Thus for injection seeding to be highly successful, the seeded pulse should continue to extract the energy from the pump pulse as fast as it arrives at the crystal. A third difference exists in the saturation effect. In a solid-state laser the laser pulse extracts the energy stored in the upper laser level to the point where the gain falls to zero. However, in an optical parametric oscillator, the gain may not fall to zero in the presence of the seeded pulse. A nonzero gain allows the unseeded modes to continue to extract energy from the pump and thus decrease the efficiency of the seeding process.

In doubly resonant optical parametric oscillators, spectral output of the device may be unstable due to an effect referred to as the cluster effect. If both the signal and idler are resonant, oscillation can only occur at frequencies that satisfy both the conservation of energy and the resonance condition. Because of these simultaneous requirements, the frequencies that oscillate may not occur at the minimum phase mismatch as shown in Fig. 23. By operating away from the point of minimum phase mismatch, the output can be significantly reduced. Worse still, the

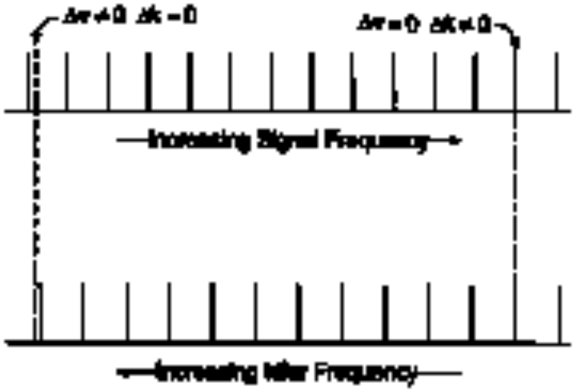

FIGURE 23 Cluster effects in doubly resonant oscillators.

different set of frequencies that satisfies both the resonance conditions and the conservation of energy can vary on a shot-to-shot basis. For example, the pump frequency may experience small variations caused by small variations in the level of excitation of the pump laser. A small variation in the pump frequency may cause a much larger difference in the frequencies that satisfy both the conservation of energy and the resonance condition. Due to instabilities associated with the cluster effect, the doubly resonant optical parametric oscillator is often avoided.

REFERENCES

1. J. A. Giordmaine and R. C. Miller, "Tunable Coherent Parametric Oscillation in $LiNbO_3$ at Optical Frequencies," *Phys. Rev. Lett.* 14, 973–976 (1965).
2. J. A. Armstrong, N. Bloembergen, J. Ducuing, and P. S. Pershan, "Interactions between Light Waves in a Nonlinear Dielectric," *Phys. Rev.* 127, 1918–1939 (1962).
3. G. D. Boyd and D. A. Kleinman, "Parametric Interaction of Focused Gaussian Light Beams," *J. Appl. Phys.* 39, 3597–3639 (1968).
4. S. E. Harris, "Tunable Optical Parametric Oscillators," *Proc. IEEE* 57, 2096–2113 (1969).
5. S. J. Brosnan and R. L. Byer, "Optical Parametric Oscillator Threshold and Linewidth Studies," *IEEE J. Quantum Electron.* QE-15, 415–431 (1979).
6. R. L. Byer and S. E. Harris, "Observation of Tunable Optical Parametric Fluorescence," *Phys. Rev. Lett.* 18, 732–734 (1967).
7. N. P. Barnes and V. J. Corcoran, "Acceptance Angles and Spectral Bandwidths of Nonlinear Interactions," *Appl. Opt.* 15, 696–699 (1976).
8. N. P. Barnes, "Tunable Mid Infrared Sources Using Second Order Nonlinearities," *Int. J. Nonlinear Opt.* 1, 639–672 (1992).
9. P. N. Butcher, *Nonlinear Optical Phenomena*, Bulletin 200 Ohio State University, Columbus, OH (1965).
10. M. Born and E. Wolf, *Principles of Optics*, Pergamon Press, New York (1964).
11. F. Zernike and J. E. Midwinter, *Applied Nonlinear Optics*, Wiley, New York (1973).

12. J. A. Armstrong, N. Bloembergen, J. Ducuing, and P. S. Pershan, "Interactions Between Light Waves in a Nonlinear Dielectric," *Phys. Rev.* 127, 1918–1939 (1962).
13. G. D. Boyd and D. A. Kleinman, "Parametric Interactions of Focused Gaussian Light Beams," *J. Appl. Phys.* 39, 3597–3639 (1968).
14. R. A. Baumgartner and R. L. Byer, "Optical Parametric Amplification," *IEEE J. Quantum Electron.* QE-15, 432–444 (1979).
15. N. P. Barnes, D. J. Gettemy, J. R. Hietanen, and R. A. Iannini, "Parametric Amplification in $AgGaSe_2$," *Appl. Opt.* 28, 5162–5168 (1989).
16. S. J. Brosnan and R. L. Byer, "Optical Parametric Oscillator Threshold and Linewidth Studies," *IEEE J. Quantum Electron.* QE-15, 415–431 (1979).
17. N. P. Barnes, K. E. Murray, J. R. Hietanen, and R. A. Iannini, "Er:YLF Pumped $AgGaSe_2$ Optical Parametric Oscillator," in *Proc. OSA Advanced Solid State Lasers*, OSA, Washington, DC 522–530 (1990).
18. S. J. Brosnan and R. L. Byer, "Optical Parametric Oscillator Threshold and Linewidth Studies," *IEEE J. Quantum Electron.* QE-15, 415–431 (1979).
19. N. P. Barnes, J. A. Williams, J. C. Barnes, and G. E. Lockard, "A Self Injection Locked Q-Switched Line Narrowed $Ti:Al_2O_3$ Laser," *IEEE J. Quantum Electron.* 24, 1021–1028 (1988).
20. G. D. Boyd, A. Ashkin, J. M. Dziedzic, and D. A. Kleinman, "Second Harmonic Generation of Light with Double Refraction," *Phys. Rev.* 137, A1305–A1320 (1965).
21. S. J. Brosnan and R. L. Byer, "Optical Parametric Oscillator Threshold and Linewidth Studies," *IEEE J. Quantum Electron.* QE-15, 415–431 (1979).
22. M. Okada and S. Ieiri, "Influences of Self-Induced Thermal Effects on Phase Matching in Nonlinear Optical Crystals," *IEEE J. Quantum Electron.* QE-7, 560–563 (1971).
23. N. P. Barnes, R. C. Eckhardt, D. J. Gettemy, and L. B. Edgett, "Heating Effects in Second Harmonic Generation," in *LTS Infrared Exchange Meeting*, Albuquerque, NM (May 1977).
24. D. T. Hon and H. Brusselbach, "Beam Shaping to Suppress Phase Mismatch in High Power Second Harmonic Generation," *IEEE J. Quantum Electron.* QE-16, 1356–1364 (1980).
25. D. Eimerl, "The Potential for Efficient Frequency Conversion at High Average Power Using Solid State Nonlinear Optical Materials," UCID-20565, University of California, (Oct. 1985).
26. T. D. Gustafson and C. L. Tang, "CW Parametric Scattering in ADP with Strong Absorption in the Idler Band," *Appl. Phys. Lett.* 12, 375–378 (1968).
27. J. D. McMullen, "Optical Parametric Interactions in Isotropic Materials Using a Phase Corrected Stack of Nonlinear Dielectric Plates," *J. Appl. Phys.* 46, 3076–3081 (1975).
28. F. Zernike and J. E. Midwinter, *Applied Nonlinear Optics*, Wiley, New York (1973).
29. V. G. Dmitriev, G. G. Gurzadyan, and D. N. Nikogosyan, *Handbook of Nonlinear Optical Crystals*, Springer Verlag, New York (1991).
30. M. J. Weber, *Handbook of Laser Science and Technology*, Vol. III, *Optical Materials*, CRC Press, Boca Raton, FL (1986).
31. M. M. Choy and R. L. Byer, "Accurate Second Order Susceptibility Measurements of Visible and Infrared Nonlinear Crystals," *Phys. Rev. B* 14, 1693–1706 (1976).
32. R. C. Eckardt, H. Masuda, Y. X. Fan, and R. L. Byer, "Absolute and Relative Nonlinear Optical Coefficients of KDP, KD*P, BaB_2O_4, $LiIO_3$, $MgO:LiNbO_3$, and KTP Measured by Phase Matched Second-Harmonic Generation," *IEEE J. Quantum Electron.* QE-26, 922–933 (1990).
33. I. H. Malitson and M. J. Dodge, "Refractive Index and Birefringence of Synthetic Sapphire," *J. Opt. Soc. Am.* 62, 1405 (1972).
34. F. Zernike, "Refractive Indices of Ammonium Dihydrogen Phosphate and Potassium Dihydrogen Phosphate Between 2000Å and 1.5 μm," *J. Opt. Soc. Am.* 54, 1215–1220 (1964).
35. L. G. DeShazer and K. E. Wilson, "Refractive Index and Thermo-Optic Coefficients of CD*A," in *Basic Properties of Optical Materials Symp.*, NBS Special Publication 574, Gaithersburg, MD (1980).
36. G. D. Boyd, W. L. Bond, and H. L. Carter, "Refractive Index as a Function of Temperature in $LiNbO_3$," *J. Appl. Phys.* 38, 1941 (1967).

37. D. Eimerl, L. Davis, and S. Velsko, E. K. Graham, and A. Zalkin, "Optical, Mechanical, and Thermal Properties of Barium Borate," *J. Appl. Phys.* 62, 1968–1983 (1987).
38. C. Chen, Y. Wu, A. Jiang, B. Wu, G. You *et al.*, "New Nonlinear-Optical Crystal: LiB_3O_5," *J. Opt. Soc. Am. B* 6, 616–621 (1989).
39. T. Y. Fan, C. E. Huang, B. Q. Hu, R. C. Eckardt, Y. X. Fan, R. L. Byer, and R. S. Feigelson, "Second Harmonic Generation and Accurate Index of Refraction Measurements in Flux-Grown $KTiOPO_4$," *Appl. Opt.* 26, 2390–2394 (1987).
40. G. D. Boyd, H. Kasper, and J. H. McFee, "Linear and Nonlinear Optical Properties of $AgGaS_2$, $CuGaS_2$, and $CuInS_2$, and Theory of the Wedge Technique for the Measurement of Nonlinear Coefficients," *IEEE J. Quantum Electron.* QE-7, 563–573 (1971).
41. G. D. Boyd, H. M. Kasper, J. H. McFee, and F. G. Storz, "Linear and Nonlinear Optical Properties of Some Ternary Selenides," *IEEE J. Quantum Electron.* QE-8, 900–908 (1972).
42. R. L. Herbst and R. L. Byer, "Efficient Parametric Mixing in CdSe," *Appl. Phys. Lett.* 19, 527–530 (1971).
43. G. D. Boyd, E. Buehler, and F. G. Storz, "Linear and Nonlinear Optical Properties of $ZnGeP_2$ and CdSe," *Appl. Phys. Lett.* 18, 301–304 (1971).
44. J. D. Feichtner and G. W. Roland, "Optical Properties of a New Nonlinear Optical Material: Tl_3AsSe_3," *Appl. Opt.* 11, 993–998 (1972).
45. N. P. Barnes, D. J. Gettemy, and R. S. Adhav, "Variation of the Refractive Indices with Temperature and the Tuning Rate for KDP Isomorphs," *J. Opt. Soc. Am.* 72, 895–898 (1982).
46. L. G. DeShazer, C. A. Hoefer, and K. W. Kirby, "Optical Characterization of Nonlinear Crystals," Final Report to Lawrence Livermore National Laboratory, Livermore, CA (1985).
47. D. J. Gettemy, W. C. Harker, G. Lindholm, and N. P. Barnes, "Some Optical Properties of KTP, $LiIO_3$, and $LiNbO_3$," *IEEE J. Quantum Electron.* QE-24, 2231–2237 (1988).
48. R. L. Herbst, "Cadmium Selenide Infrared Parametric Oscillator," Microwave Laboratory Report 2123, Stanford University, Stanford, CA (1972).
49. M. D. Ewbank, P. R. Newman, N. L. Mota, S. M. Lee, W. L. Wolfe *et al.*, "The Temperature Dependence of Optical and Mechanical Properties of Tl_3AsSe_3," *J. Appl. Phys.* 51, 3848–3852 (1980).
50. J. A. Giordmaine and R. C. Miller, "Tunable Coherent Parametric Oscillation in $LiNbO_3$ at Optical Frequencies," *Phys. Rev. Lett.* 14, 973–976 (1965).
51. R. G. Smith, J. E. Geusic, H. J. Levinstein, J. J. Rubin, S. Singh, and L. G. Van Uitert, "Continuous Optical Parametric Oscillation in $Ba_2NaNb_5O_{15}$," *Appl. Phys. Lett.* 12, 308–310 (1968).
52. R. L. Byer, M. K. Oshman, J. F. Young, and S. E. Harris, "Visible CW Parametric Oscillator," *Appl. Phys. Lett.* 13, 109–111 (1968).
53. L. B. Kreuzer, "High Efficiency Optical Parametric Oscillation and Power Limiting in $LiNbO_3$," *Appl. Phys. Lett.* 13, 57–59 (1968).
54. J. E. Bjorkholm, "Efficient Optical Parametric Oscillation Using Doubly Resonant and Singly Resonant Cavities," *Appl. Phys. Lett.* 13, 53–56 (1968).
55. J. M. Yarborough and G. A. Massey, "Efficient High Gain Parametric Generation in ADP Continuously Tunable across the Visible Spectrum," *Appl. Phys. Lett.* 18, 438–440 (1971).
56. R. L. Herbst, R. N. Fleming, and R. L. Byer, "A 1.4–4.0 µm High Energy Angle Tuned $LiNbO_3$ Parametric Oscillator," *Appl. Phys. Lett.* 25, 520–522 (1974).
57. R. L. Herbst and R. L. Byer, "Singly Resonant CdSe Infrared Parametric Oscillator," *Appl. Phys. Lett.* 21, 189–191 (1972).
58. J. A. Weiss and L. S. Goldberg, "Singly Resonant CdSe Parametric Oscillator Pumped by an HF Laser," *Appl. Phys. Lett.* 24, 389–391 (1974).
59. T. Kushida, Y. Tanaka, and M. Ojima, "Tunable Picosecond Pulse Generation by Optical Parametric Oscillator," *Jpn. J. Appl. Phys.* 16, 2227–2235 (1977).
60. G. P. Arnold, N. P. Barnes, and D. J. Gettemy, and R. G. Wenzel, "Anomalous Behavior of Some Synchronously Pumped Mode Locked Parametric Oscillators," in *Lasers '80*, New Orleans, LA (Dec. 1980).

61. R. C. Eckhardt, Y. X. Fan, R. L. Byer, C. L. Marquardt, M. E. Storm, and L. Esterowitz, "Broadly Tunable Infrared Parametric Oscillator Using $AgGaSe_2$," *Appl. Phys. Lett.* **49,** 608–610 (1986).
62. W. R. Bosenberg, W. S. Pelouch, and C. L. Tang, "High Efficiency and Narrow Linewidth Operation of a Two Crystal β–BaB_2O_4 Optical Parametric Oscillator," *Appl. Phys. Lett.* **58,** 1461–1463 (1991).
63. Y. Wang, Z. Xu, D. Deng, W. Zheng, X. Liu *et al.*, "Highly Efficient Visible and Infrared β–BaB_2O_4 Optical Parametric Oscillator With Pump Reflection," *Appl. Phys. Lett.* **58,** 1461–1463 (1991).
64. S. Chandra, M. J. Ferry, and G. Daunt, "115 mJ, 2-Micron Pulses by OPO in KTP," in *Advanced Solid State Laser Conf.*, Santa Fe, NM (Feb. 1992).
65. V. L. Boichenko, M. M. Novikov, and A. I. Kholodnykh, "Improvement in the Output Characteristics of a Pulsed Optical Parametric Oscillator on Injection of an External Signal into an Extracavity Wave," *Sov. J. Quant. Elect.* **17,** 392–393 (1987).
66. W. R. Bosenberg, D. R. Guyer, and C. E. Hamilton, "Single Frequency Optical Parametric Oscillators," in *CLEO Conf.*, Baltimore, MD (May, 1993).
67. N. P. Barnes, G. H. Watson, and K. E. Murray, "Injection Seeded Optical Parametric Oscillator," in *Advanced Solid State Laser Conf.*, Santa Fe, NM (Feb. 1992).